Theses and Dissertations   1. Thesis and Dissertation Collection, all items

1977-06

Initial unsteady aerodynamic measurements of a circulation controlled airfoil and an oscillating flow wind tunnel.

Lancaster, Emmet John

Monterey, California. Naval Postgraduate School

http://hdl.handle.net/10945/18154

INITIAL UNSTEADY AERODYNAMIC MEASUREMENTS
OF A CIRCULATION CONTROLLED AIRFOIL AND AN
OSCILLATING FLOW WIND TUNNEL

Emmett John Lancaster

NAVAL POSTGRADUATE SCHOOL
Monterey, California

THESIS

INITIAL UNSTEADY AERODYNAMIC MEASUREMENTS
OF A CIRCULATION CONTROLLED AIRFOIL AND AN
OSCILLATING FLOW WIND TUNNEL

by

Emmett John Lancaster

June 1977

Thesis Advisor: L. V. Schmidt

T178650

REPORT DOCUMENTATION PAGE		READ INSTRUCTIONS BEFORE COMPLETING FORM
1. REPORT NUMBER	2. GOVT ACCESSION NO.	3. RECIPIENT'S CATALOG NUMBER
4. TITLE (and Subtitle) Initial Unsteady Aerodynamic Measurements of A Circulation Controlled Airfoil and an Oscillating Flow Wind Tunnel		5. TYPE OF REPORT & PERIOD COVERED Master's Thesis; June 1977
		6. PERFORMING ORG. REPORT NUMBER
7. AUTHOR(s) Emmett John Lancaster		8. CONTRACT OR GRANT NUMBER(s)
9. PERFORMING ORGANIZATION NAME AND ADDRESS Naval Postgraduate School Monterey, California 93940		10. PROGRAM ELEMENT, PROJECT, TASK AREA & WORK UNIT NUMBERS
11. CONTROLLING OFFICE NAME AND ADDRESS Naval Postgraduate School Monterey, California 93940		12. REPORT DATE June 1977
		13. NUMBER OF PAGES 73
14. MONITORING AGENCY NAME & ADDRESS(if different from Controlling Office)		15. SECURITY CLASS. (of this report) Unclassified
		15a. DECLASSIFICATION/DOWNGRADING SCHEDULE

16. DISTRIBUTION STATEMENT (of this Report)

Approved for public release; distribution unlimited.

17. DISTRIBUTION STATEMENT (of the abstract entered in Block 20, if different from Report)

18. SUPPLEMENTARY NOTES

19. KEY WORDS (Continue on reverse side if necessary and identify by block number)

20. ABSTRACT (Continue on reverse side if necessary and identify by block number)

Steady state results of lift developed by varying the momentum blowing coefficient (C_μ) upon a refurbished Circulation Control Rotor (CCR) airfoil section were favorable. This thesis was an experimental investigation to quantitatively evaluate whether the steady state results could be applied by a quasi-steady assumption when a harmonic perturbation of C_μ was

DD FORM 1473 EDITION OF 1 NOV 65 IS OBSOLETE
1 JAN 73

S/N 0102-014-6601 |

1

superimposed upon the steady value. Results suggested an attenuation in the dynamic transfer function of dC_p/dC_μ as the oscillating blowing frequency was increased.

The oscillating flow wind tunnel in which the CCR airfoil section was tested exhibited a relationship between pressure and velocity amplitude not in accordance with quasi-steady small perturbation theory. Initial measurements indicated that the RMS C_p perturbation was an order of magnitude greater than the normalized RMS velocity perturbation. To further clarify this situation, investigations were conducted to establish a dynamic frequency response calibration of the wind tunnel. Results confirmed the order of magnitude difference between the RMS C_p and normalized RMS velocity perturbations, indicating that the tunnel flow environment was governed by Euler's equation in its complete form rather than with the simplifications which lead to the quasi-steady small perturbation theory.

Initial Unsteady Aerodynamic Measurements
of A Circulation Controlled Airfoil and an
Oscillating Flow Wind Tunnel

by

Emmett John Lancaster
Lieutenant, United States Navy
B.S., United States Naval Academy, 1970

Submitted in partial fulfillment of the
requirements for the degree of

MASTER OF SCIENCE IN AERONAUTICAL ENGINEERING

from the

NAVAL POSTGRADUATE SCHOOL
June   1977

ABSTRACT

Steady state results of lift developed by varying the momentum blowing coefficient (C_μ) upon a refurbished Circulation Control Rotor (CCR) airfoil section were favorable. This thesis was an experimental investigation to quantitatively evaluate whether the steady state results could be applied by a quasi-steady assumption when a harmonic perturbation of C_μ was superimposed upon the steady value. Results suggested an attenuation in the dynamic transfer function of dC_p/dC_μ as the oscillating blowing frequency was increased.

The oscillating flow wind tunnel in which the CCR airfoil section was tested exhibited a relationship between pressure and velocity amplitude not in accordance with quasi-steady small perturbation theory. Initial measurements indicated that the RMS C_p perturbation was an order of magnitude greater than the normalized RMS velocity perturbation. To further clarify this situation, investigations were conducted to establish a dynamic frequency response calibration of the wind tunnel. Results confirmed the order of magnitude difference between the RMS C_p and normalized RMS velocity perturbations, indicating that the tunnel flow environment was governed by Euler's equation in its complete form rather than with the simplifications which lead to the quasi-steady small perturbation theory.

TABLE OF CONTENTS

LIST OF TABLES

LIST OF ILLUSTRATIONS

Figure

LIST OF SYMBOLS AND ABBREVIATIONS

Symbol/Abbreviation   Definition

a   Speed of sound

atm   Atmosphere

c   Wave propagation velocity
                  $c = (a - U)$ upstream and $(a + U)$ downstream

CCR   Circulation Control Rotor

chnl   Channel

C_L Lift coefficient

C_p Pressure coefficient

$$C_p = \frac{P_x - P_{REF}}{g}$$

C_μ Momentum blowing coefficient

$$C_\mu = \frac{\dot{M}U_j}{qS}$$

e_{HW} Hot wire voltage

I.D.   Inside diameter

$\dot{M}$ Steady state or mean mass flow rate
                  (see subscripts)

$\dot{m}$ Mass flow rate perturbation

P   Steady state or mean pressure (see sub-
                  scripts)

p   Pressure perturbation

q   Dynamic pressure

$$q = \tfrac{1}{2}\rho U_o^2$$

RMS   Root mean square

S   CCR airfoil section wing area

9

S/V	Scanivalve
U	Steady state or mean velocity (see subscripts)
u	Velocity perturbation
upstrm	Upstream
wingsta	Wing station (main test station)
x/c	Chordwise direction in percent of chord 0 at leading edge to 1.0 at training edge
x-ducer	Transducer
ε, σ	Perturbation oscillation amplitude in percent of mean value
θ	Angular measurement from slot clockwise around trailing edge
ρ	Density
ϕ	Phase angle also Velocity potential in tunnel frequency response results discussion

Subscripts

HW	hot wire
j	Coanda jet
m	Mean
o	Steady state
RMS	Root mean square
s	Static
t	Total

ACKNOWLEDGEMENT

The author wishes to express his appreciation to
Dr. Louis V. Schmidt, LT Karl A. Kail, John A. Mounton, and
Gloria, Bryan and Eric without whose encouragement, patience,
and understanding this thesis would not have been possible,

I. INTRODUCTION

The purpose of the Circulation Control Rotor (CCR) blade is to modulate the lift (circulation) of the blade utilizing the Coanda principle. As the blade travels about the rotor hub, the lift is modulated azimuthally by varying the amount of air blown out of a slot above the blade trailing edge, as shown in Figure 1.

Steady state results of lift developed by varying the momentum blowing coefficient of a CCR airfoil section were promising (see Figure 16). It was the primary purpose of this thesis to quantitatively evaluate whether the steady state results were valid when a harmonic perturbation of momentum blowing coefficient was superimposed upon the steady value, as it would be in the helicopter rotor blade environment.

During the majority of time available for thesis research, the prototype Lockheed-fabricated CCR airfoil section was removed from the tunnel, undergoing extensive rework and calibration to correct slot irregularities and pressure orifice discrepancies [10]. This provided an opportunity to perform calibrations upon the oscillating flow field of the wind tunnel using pressure transducers and a hot wire anemometer.

Unsteady measurements taken prior to airfoil section rework [10] showed that when

$$u(t) = U_0 (1 + \varepsilon \cos \omega t)$$
$$\varepsilon = 0.107, \quad \frac{\langle u^2 \rangle^{1/2}}{U_0} = 0.075$$

the RMS C_p obtained using linearized theory was

$$\langle C_p^2 \rangle^{\frac{1}{2}} \cong 2.0$$

uniform and approximately in phase over the complete airfoil at $f = 62$ Hz, $U_O = 105$ fps. Quasi-steady small perturbation theory states that

$$\langle C_p^2 \rangle^{\frac{1}{2}} = 2 \frac{\langle u^2 \rangle^{\frac{1}{2}}}{U_o}$$

which was not in accordance with the results experimentally observed. Clearly, since there is an order of magnitude difference between $\langle C_p^2 \rangle^{\frac{1}{2}}$ and $\frac{\langle U^2 \rangle^{\frac{1}{2}}}{U_o}$, quasi-steady small perturbation theory appeared to be an invalid assumption in this tunnel flow environment.

It was the secondary purpose of this thesis to perform a tunnel dynamic frequency response calibration to further clarify the tunnel flow environment's discord with quasi-steady small perturbation theory. In accordance with this purpose, tunnel frequency response measurements of both RMS pressure and velocity perturbations were experimentally obtained.

CIRCULATION CONTROL ROTOR HUB/VALVE

KAMAN

COLLECTIVE PITCH CONTROL →

BLADE DUCT →

FLEX RING

AIR

→ TRANSMISSION

ELLIPTICAL AIRFOIL

THIN FILM OF AIR ADHERES TO
ROUNDED TRAILING EDGE BY
THE COANDA EFFECT INDUCING
CIRCULATION & CREATING
HIGH LIFT

DIRECTION OF ROTATION

ROTOR BLADE OPERATES IN FIXED PITCH

CONTROL AIR EXITS FROM CONTINUOUS
TRAILING EDGE SLOT

CYCLIC CONTROL OF AIRFLOW GENERATES
CYCLIC CONTROL OF LIFT

KAMAN AEROSPACE CORPORATION
A KAMAN COMPANY

NAVAL AIR SYSTEMS COMMAND
NAVAL SHIP R&D CENTER

Figure 1. Circulation Control Rotor concept

14

II.   EXPERIMENTAL EQUIPMENT AND PROCEDURES

A.   METHOD OF INVESTIGATION

1.   Wind Tunnel Frequency Response Calibration

The experiment conducted was an evaluation of the frequency response for the oscillating flow wind tunnel. The quantities which were measured were RMS static and total pressure perturbations, RMS velocity perturbation, and the phase angle between total pressure perturbations at two different tunnel locations. The major equipment used to collect and measure data are portrayed schematically in Figure 7. In addition to the above data collected, polaroid pictures were taken of representative oscilloscope traces of time histories for the measured quantities.

The raw data collected were RMS voltmeter readings, DC level voltmeter readings, phasemeter phase angle readings and polaroid pictures. The tabular raw data are presented in Table III. The oscilloscope pictures are presented in Figures 12 and 13.

The raw data were reduced using the method presented in the calibration section, II.B.3, for the velocity perturbation and in Figures 26 and 27 for the pressure perturbations. The reduced results are presented graphically in Figures 10, 11, and 14.

2.   CCR Airfoil Section Tests

The tests conducted were to determine quantitatively whether the steady state dC_L/dC_μ was valid when a harmonic

modulation of momentum blowing coefficient was superimposed upon the steady value. The major equipment and test arrangement are portrayed schematically in Figure 8.

The quantities measured were CCR airfoil surface pressures, CCR plenum cavity static pressure, plenum cavity air supply pipe velocity, and mass flow rate. The raw data collected were RMS voltmeter readings, DC level voltmeter readings, rotameter mass flow rate readings, and polaroid pictures of representative oscilloscope traces.

The raw data were reduced as described by Schmidt [10] and Kail [6]. The surface static pressure data were manually transferred from the printer tape to an HP 9830 calculator cassette tape for numerical integration of the pressure distributions. The HP 9830 was preprogrammed to calculate C_L, C_D, C_M about the 0.25 chord, and C_μ (the momentum blowing coefficient). The calculation of C_μ[1] depended upon the Coanda air mass flow rate and slot jet velocity. The reduced results are presented graphically in Figures 21 and 22. The oscilloscope traces are presented in Figures 24 and 25.

_____

[1]The method used for calculating C_μ is explained in the discussion of results section, III.B.
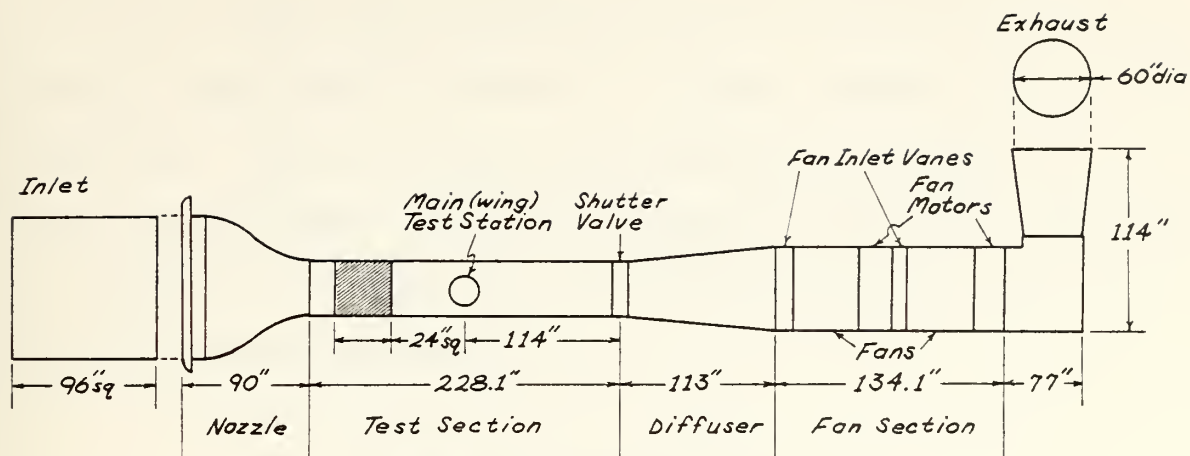
Figure 2. Plan view of wind tunnel

B. DESCRIPTION OF APPARATUS AND PROCEDURES

   1. Description of Experimental Apparatus and
       Instrumentation

      a. Wind Tunnel

      All data were collected using the low-speed,
oscillating flow wind tunnel located in the Aeronautics
Laboratories of the Naval Postgraduate School. The basic
tunnel layout and dimensions are shown in Figure 2. The
entire tunnel, with the exception of the test section, was
constructed of one-quarter inch steel plate, the heavy
construction necessary to withstand the induced vibrations
of the oscillating flow. Three high solidity screens were
located in the inlet section for reduction of test section
turbulence. The screens were pre-tensioned by spring loaded
frames, recessed into the walls of the inlet. The nozzle
section of the tunnel has a contraction ratio of 16:1.
The screens and contraction ratio produce test section free
stream turbulence levels of 0.3 to 0.4 percent [8].

17

The tunnel was driven by two Joy Axivane fans in series. Each fan was driven by a direct connect 100 hp, 1750 rpm motor. The fan blades were adjustable through a 25 to 55 degree pitch range. Directly in front of each fan was a set of variable inlet vanes for maintaining external control of the test section velocity.
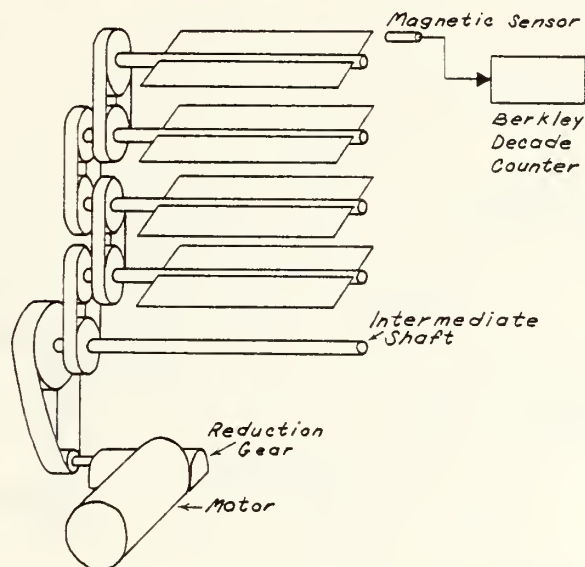
Figure 3. Wind Tunnel Rotating Shutter

b. Rotating Shutter Valve

The rotating shutter valve shown in Figure 3 consisted of four equally spaced rotating shafts. Each shaft was crosscut down its entire length with a one-quarter inch slot into which fit a one-quarter inch flat aluminum plate (blade). Two, three, four, and five-inch blades could be used to obtain oscillation amplitudes of from 8 to 92 percent of the free stream velocity [8]. The shutter shafts were driven by a five horsepower variable speed electric motor through

18

an intermediate shaft. A wide variety of pulley ratios
could be employed to obtain oscillation frequencies of from
2 to 933 Hz [8].

The oscillation frequency was measured using a
magnetic pickup; the output was read from a Berkeley decade
counter.

c. Tunnel Test Section
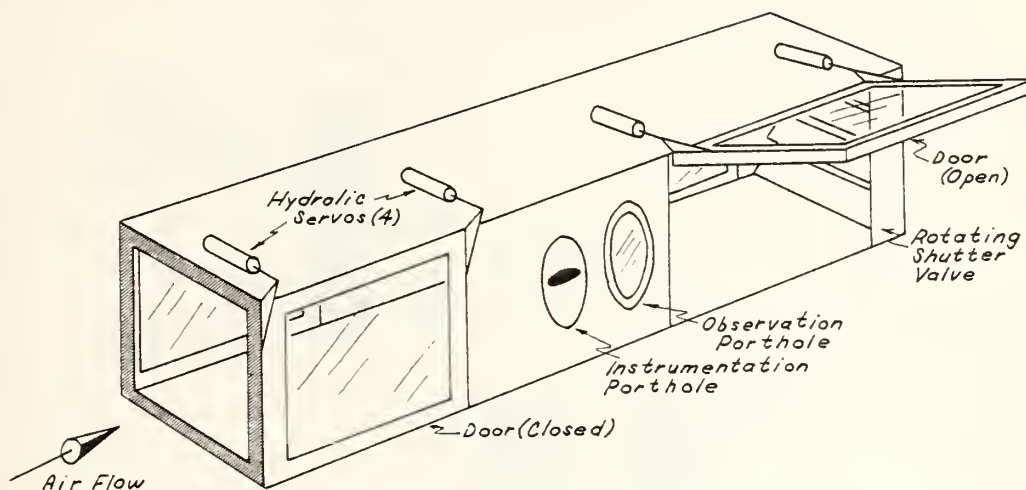
Figure 4. Wind Tunnel Test Section

The 18-foot long wind tunnel test section is
shown in Figure 4. The top and bottom of the test section
were single-piece two-inch thick aluminum plates. Each side
of the test section consisted of three separate 74.5 inch
long sections. The fore and aft sections on each side were
two-inch thick stress-relieved lucite plate. The lucite
plates on the operator side of the test section were con-
structed as doors, raised and lowered by hydraulically
actuated servos. The middle section of each side was con-
structed of two-inch thick plywood. In the middle of each

19

plywood section was a 16-inch porthole to accept apparatus
to be tested in the tunnel. Immediately downstream of the
instrumentation porthole on the operator side of the tunnel
was a 16-inch diameter, two-inch thick lucite observation
porthole.

> d. Test Section Instrumentation
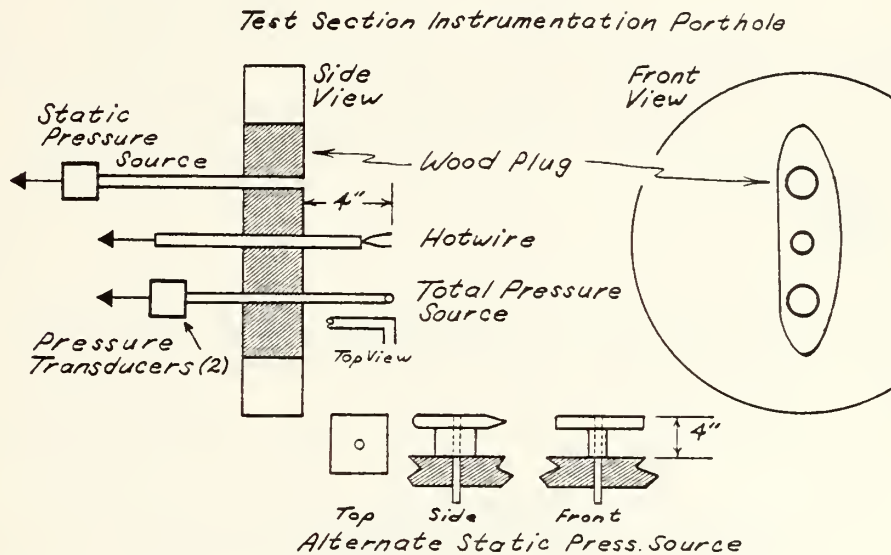
Figure 5. Instrumentation for Frequency
Response Calibration

The wind tunnel instrumentation package for the
frequency response calibration consisted of a total pressure
source, a static pressure source, and a hot wire anemometer.
The instrumentation was mounted in a wooden plug which was
mounted in the hole cut for the CCR airfoil section, as
shown in Figure 5. A wooden plug containing no instrumenta-
tion was mounted into the instrumentation porthole on the
opposite side of the test section. In addition, two total
pressure sources were located upstream from the main

20

instrumentation station: one in the test section floor
used for adjusting test section velocity, and one 34 inches
upstream in the test section wall at the same height as the
main station total pressure source, used in lieu of the sta-
tic pressure source. The total pressure source at 34 inches
upstream was used to make a comparison with the main instru-
mentation station total pressure source.
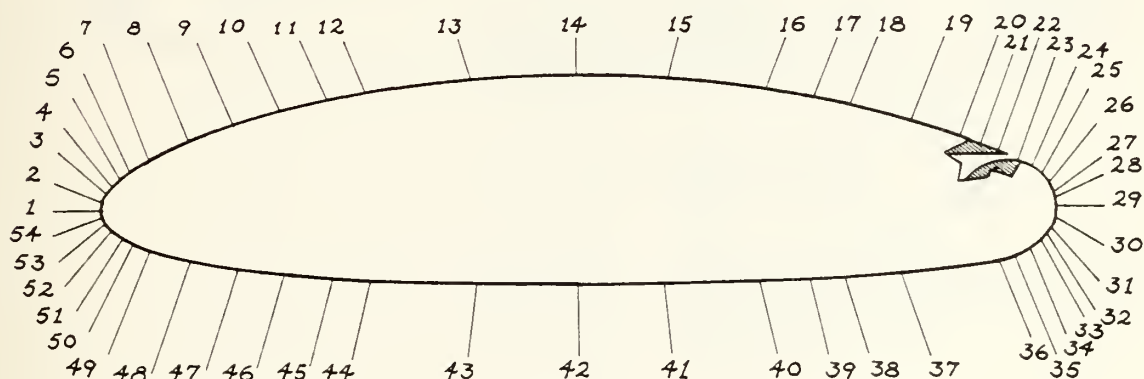
Figure 6.   CCR Airfoil Section Static Pressure
Port Locations

        The pressure sensing system used to collect data
from the CCR airfoil section is shown schematically in Figure
8. The pressure tap locations are shown in Figure 6 and are
listed in Table I. The pressure sensing system employed
uniform lengths of 0.0331 inch I.D. steel tubing connecting
the airfoil surface static pressure ports with the scanivalves.
Two scanivalves were employed: one 24 channel and one 48
channel.

        The static pressure in the airfoil section plenum
cavity was also monitored. The steady state value was

21
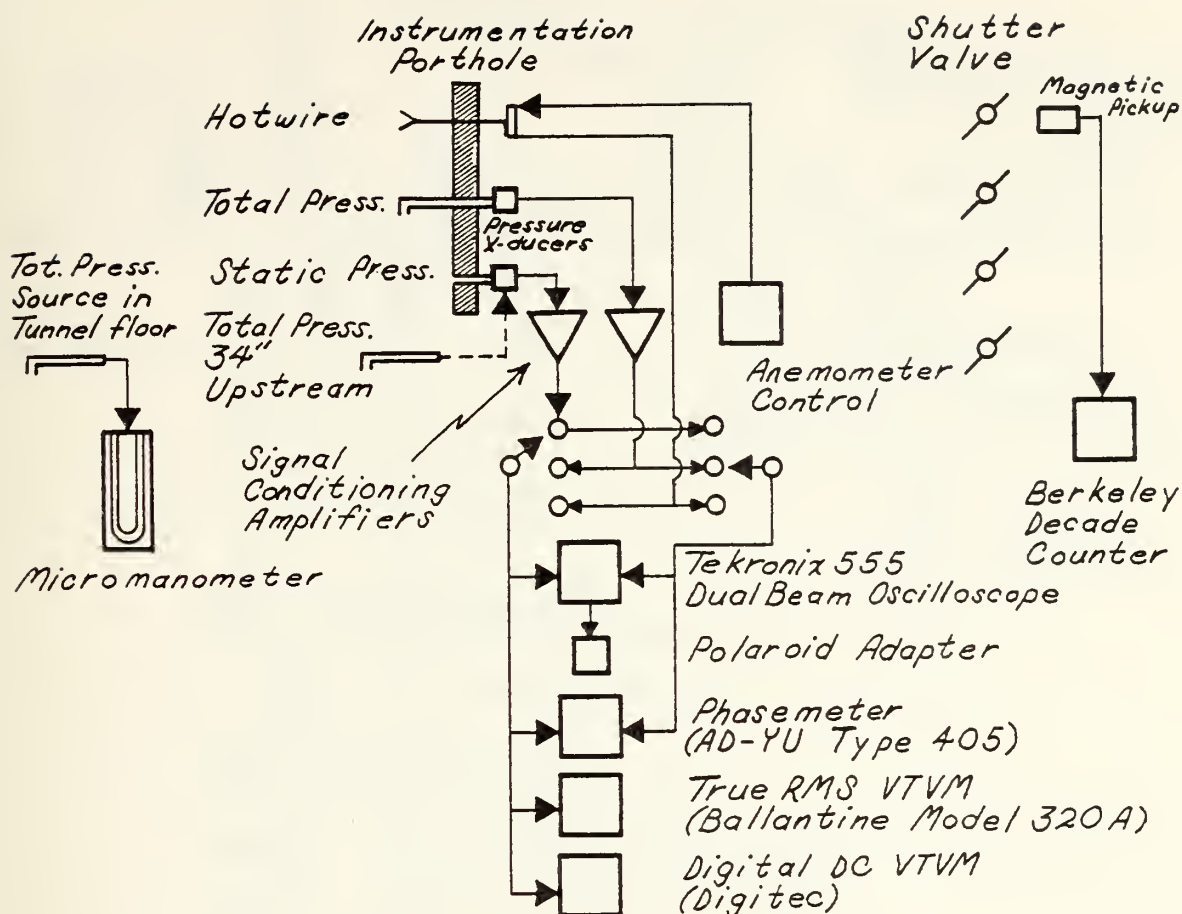
Figure 7.   Frequency Response Calibration
Equipment Schematic

measured using a manometer, and the oscillating perturbation

was measured using a pressure transducer of the type installed

in the scanivalves.

    e.   Raw Data Measurement Equipment

        The raw data for the frequency response calibra-

tion were collected by the equipment shown schematically in

Figure 7.   The instrumentation and measurement equipment for

CCR airfoil raw data collection are shown schematically in
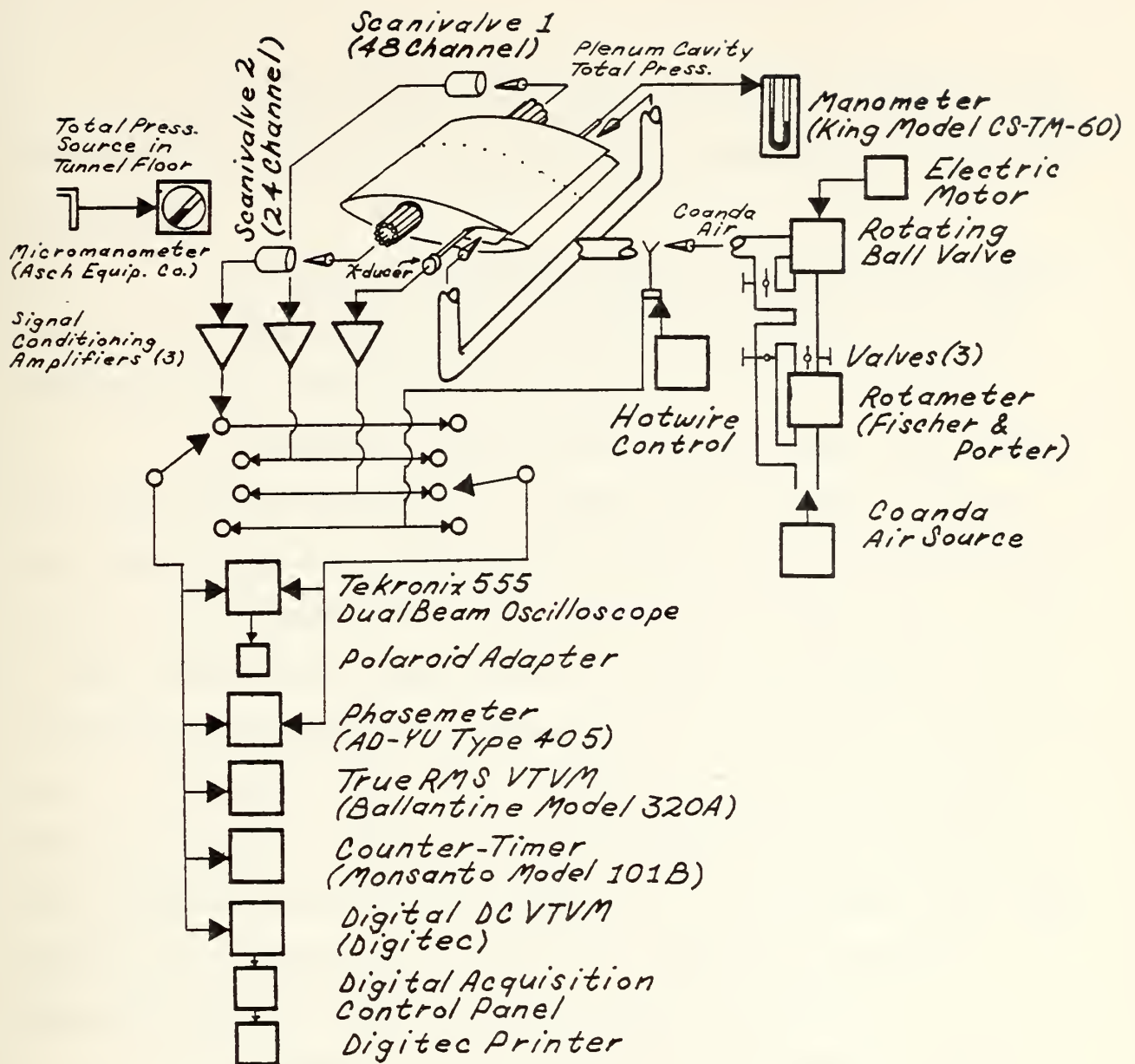
Figure 8.

Figure 8. CCR Airfoil Section
Equipment Schematic

The dual-beam oscilloscope was used to display
the time variant response of any of the measured quantities.
It was also equipped with a polaroid adapter for pictorially
recording ocsilloscope traces.

The true RMS voltmeter was used to obtain RMS
readings of any oscillating data.

The phasemeter was used to obtain the phase angle difference between any two quantities oscillating at the same frequency.

The digital voltmeter was used to zero the signal conditioning amplifiers and to take steady state (DC level) readings of the measured quantities.

The digital acquisition control panel was linked via the digital voltmeter to a paper tape printer. The control system had the capability of cycling either automatically through the channels of either scanivalve or manually, one at a time, through any combination of scanivalve channels. All voltmeter readings were automatically printed on the printer's tape, if desired. The printer could be easily disconnected from the control system cycling processes. The cycling rate was variable; however, even when set on the fastest rate, this system was inadequate to effectively sample the rapidly changing surface pressures on the airfoil section.

The Berkeley decade counter was used to obtain the frequency of the rotating shutter valve and the frequency of the oscillating velocity and pressure perturbations.

The hot wire anemometer control was used to set the hot wire current and monitor the direct current component of the output. The alternating current component of the output was displayed on the dual-beam oscilloscope. For a more complete description of the hot wire anemometer, see Miller [14].

The micromanometer was used to set and adjust the desired test section velocity. Its 33 foot tubing length was sufficient to completely damp out the oscillating pressure perturbations.

The counter-timer was used to measure the frequency of the momentum blowing coefficient when it was being oscillated. The oscillating quantities input into the counter-timer were either the plenum cavity static pressure or the hot wire velocity measured in the Coanda air supply pipe.

The rotameter was used to measure and set the mass flow rate of the Coanda air. The mass flow rate versus rotameter reading is shown in Appendix A, Figure 31.

2. How Experiments Were Conducted

The experiments were conducted utilizing the apparatus explained in the previous section. After all of the equipment had warmed up for 20 to 30 minutes, the first step was to zero the signal conditioning amplifiers for the pressure transducers and set the hot wire anemometer current. The signal conditioning amplifiers were zeroed using potentiometers and the digital DC voltmeter. The hot wire anemometer wire current was set to 30 mA, using the input mode of the anemometer control. Steady, no flow conditions were maintained in the tunnel for these initial adjustments by inserting styrofoam plugs into both ends of the tunnel test section.

After the initial adjustments were made, the styrofoam plugs were removed and the tunnel started up. The test section dynamic pressure was set to 10 psf (4.89 cm H_2O) for

the frequency response calibration and 10.2 psf (5.00 cm H_2O) for the CCR tests, using the variable inlet vanes. This resulted in a test section velocity of 92 fps for the frequency response calibration and 93 fps for the CCR tests. When the test section dynamic pressure was set, the hot wire anemometer control was switched to its output mode and the attenuation adjusted until the DC output read 1.0 V. With the above adjustments made, initial steady state DC readings of total and static pressure, and velocity, and RMS readings of pressure and velocity turbulence levels were taken.

For the frequency response calibration, the rotating shutter valve was then started, letting it run at its lowest frequency, about 9 Hz. When the shutter frequency became stabilized, it was necessary to reset the test section dynamic pressure, because of energy changes or losses in the tunnel system.

Output readings were then taken on all measured quantities at that particular frequency. The shutter frequency was then stepped up in desired increments and the measured quantity outputs recorded at each increment to a maximum frequency of about 45 Hz. Each time the frequency was stepped an increment, it was necessary to reset the test section dynamic pressure.

For the CCR airfoil section tests, the blades on the rotating shutter valve were removed. The airfoil section was then set at -5° angle of attack; -5° being the approximate zero lift angle of attack at $C_\mu = 0$ (see Figure 16).

26

After the steady pressure readings and pictures had been taken, the airfoil section air supply was turned on. The mass flow rate was adjusted to 0.58 on the rotameter, corresponding to C_μ = 0.045.[2]

It should be especially noted that the testing environment, particularly when the rotating shutter value was operating, was extremely unfavorable. This environment permitted operation for only short periods of time, even with the use of sound attenuator ear protection. When the rotating shutter valve was in operation, the tunnel could only be operated from 0900 to 1600; operation outside of these times was subject to complaints by local residents. Operating the tunnel with the rotating shutter valve going could be likened to standing beside the tracks when a freight train was speeding by.

3.   Equipment Calibrations

All transducers were statically calibrated for pressure sensitivity. All transducer and tubing length combinations were dynamically calibrated for frequency response transfer function. Dynamic calibrations were made using a method reported by Johnson [5]. Calibration results confirmed the smooth variation in both the dynamic gain function and the phase shift as the frequency was varied from 0 to 100 Hz. Separate calibrations were made for both the tunnel frequency

---

[2]This value was chosen based on information from Kaman Aerospace Corp. as being a typical C_μ value for an operational CCR helicopter.

27

response calibration and the CCR airfoil section tests. The static and dynamic transducer calibration curves are shown in Figures 26 to 30.

The hot wire anemometer was calibrated by first setting the desired test section dynamic pressure, in cm H_2O, using the micromanometer. The hot wire control was then switched to read voltage output with the attenuation set such that the output read 1.0 V at the desired test section steady velocity. Any velocity perturbations superimposed upon the steady value would then be a direct percentage of the tunnel velocity. For example: a true RMS voltmeter reading of 20.0 mV would represent an RMS velocity perturbation that was 2 percent of the original steady test section velocity.

The rotameter calibration was based on four separate tunnel runs. The resulting calibration curves are shown in Figure 31.

The airfoil pressure tap locations and corresponding scanivalve channels are listed in Tables I and II.

III. EXPERIMENTAL RESULTS AND DISCUSSION

A. WIND TUNNEL FREQUENCY RESPONSE CALIBRATION

Looking at the results of the tunnel frequency response calibration shown in Figure 10, two things are immediately apparent. The most obvious is that there are at least four resonant frequencies between 9 and 48 Hz, the primary one being about 21 Hz. The second, and not so obvious, is the nature of the velocity and pressure perturbation relationship.

To be compared with the RMS C_p, the RMS velocity perturbation was first normalized with respect to the free stream velocity. The comparison of the normalized RMS velocity and RMS C_p perturbations is shown in Figure 11, where it can be clearly seen that the RMS C_p is an order of magnitude greater than the normalized RMS velocity perturbation.

Quasi-steady small perturbation theory would conclude that

$$\langle C_p^2 \rangle^{1/2} = \frac{2 \langle u^2 \rangle^{1/2}}{U_o}$$

Clearly, since an order of magnitude difference was observed between $\langle C_p^2 \rangle^{1/2}$ and $\langle u^2 \rangle^{1/2}/U_o$, this is not the case and quasi-steady small perturbation theory is an invalid assumption in this tunnel flow environment.

The solution to the tunnel flow environment lies in analysis of Euler's equation [2, 7, 11, 13]:

$$\frac{\partial u}{\partial t} + U_o \frac{\partial u}{\partial x} = \frac{-1}{\rho} \frac{\partial P}{\partial x}$$

where U_o = free stream velocity
u = velocity perturbation
p = pressure perturbation
ρ = density

29

Using potential flow theory:

$$u = \frac{\partial \emptyset}{\partial x} = \emptyset_x$$

and d'Alembert's solution:

$$\emptyset = f(x + ct) = f(z) \text{ where } c = \text{wave propagation velocity}$$

and assuming a solution of the form:

$$u(x + ct) = u(z) = U_o \emptyset_x \text{ and } p(x + ct) = p(z)$$

then Euler's equation can be rewritten:

$$c\, U_o f'' + U_o^2 f'' = -\frac{1}{\rho}\, p'$$

$$2\left(1 + \frac{c}{U_o}\right) f'' = \frac{-1}{\frac{1}{2}\rho U_o^2}\, p'$$

Recognizing that

$$f'' = f' \emptyset_x = f' \frac{u}{U_o} \quad , \quad \frac{p'}{\frac{1}{2}\rho U_o^2} = \frac{dC_p}{dz}$$

then Euler's equation can be stated

$$\frac{d}{dz}\left[2\left(1 + \frac{c}{U_o}\right)\frac{u}{U_o} + C_p\right] = 0$$

Therefore $\langle C_p^2 \rangle^{\frac{1}{2}} = 2\left(1 + \frac{c}{U_o}\right)\frac{\langle u^2 \rangle^{\frac{1}{2}}}{U_o}$

where c = (local speed of sound) - (free stream velocity)[3]

$\quad$ c $\cong$ 1100-92 fps $\cong$ 1008 fps, then

$$\langle C_p^2 \rangle^{\frac{1}{2}} \cong 24\, \frac{\langle u^2 \rangle^{\frac{1}{2}}}{U_o}$$

Therefore, consideration of Euler's equation would imply that the RMS C_p perturbation would be an order of magnitude greater than the normalized RMS velocity perturbation at low tunnel

_____

[3] c = a - U_o for wave propagation upstream and a + U_o for wave propagation downstream.

30

mach numbers. This is clearly the situation evidenced in
Figure 11 for the tunnel flow environment.

Thus the pressure perturbation disturbance in the tunnel
may be viewed as a traveling wave emanating from the rotating
shutter valve. Because the disturbance may be viewed as a
traveling wave, it was surmised that the resonance was due
to wave reflection within the tunnel. Probable sources of
wave reflection were: the open inlet end, the inlet screens,
the rotating shutter valve, the fan section, and the down-
stream wall where the flow bends 90° just prior to exit.
Ingard and Singhal [4] experimentally investigated the effect
of flow on the acoustic resonance of an open-ended duct. They
identified several other mechanisms that may contribute to
resonance: the convection of the sound pressure pulses by
the mean flow, the interaction of sound pressure pulses with
the turbulent flow within the duct, and the effect of flow
on the reflection coefficients at the ends of the duct.

Of particular interest regarding this resonance phenomenon
was that the velocity and pressure perturbation ocsillations
achieved their smoothest, most sinusoidal profiles in the
vicinity of the maximum resonant peak, 19 to 24 Hz. This can
be seen in the oscilloscope traces of Figures 12 and 13.
Compare the traces of 23.2 Hz in Figure 12 and 19 Hz in
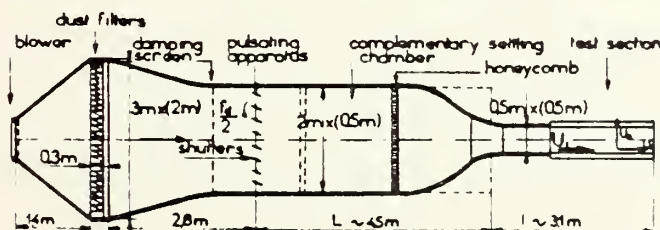
Figure 9.   Charnay & Mathieu Rotating
Shutter Wind Tunnel

Figure 13 with those at the other frequencies. Charnay and Mathieu [1] noted the same phenomenon in their rotating shutter wind tunnel, shown in Figure 9, and attribute it to when the vortex shedding frequencies of the shutter coincide with the tunnel resonance frequencies at about 20 and 60 Hz.

Also of interest in relation to tunnel resonance were the vibrational modes of the tunnel structure; around 21 Hz the tunnel structure exhibited heavy vibrations. The tunnel structural vibrations also increased at the other resonant peaks in the frequency response; however, none of the other three modes was as severe as the one at 21 Hz. Tunnel structural vibrations also varied directly as the size of the rotating shutter blades. For this reason, the 3-inch blades were used for the frequency response calibration instead of the 4-inch blades.

In an attempt to confirm that the airflow in the tunnel behaved according to the wave equation, another total pressure source was located 34 inches upstream in the tunnel wall at the same height as the total pressure source at the main test station. Initial estimates determined that at f = 22 Hz, T = 65°F(a, the speed of sound, $\cong$ 1123 fps), $U_o \cong$ 92 fps then Δt = (34/12 ft)/(1123 - 92 fps) = 2.75 ms, and $\emptyset$ = (Δt) (f) (360) $\cong$ 22°. But as can be seen from Figure 10, the phase shift between the two total pressure locations was nowhere near that value. In fact, the phase shift seems to vary inversely as the RMS pressure perturbation for frequencies

up to about 32 Hz, and then directly as the RMS pressure perturbation for higher frequencies. The phase shift may also be a function of the tunnel resonance.

Another interesting aspect that may be attributable to the resonance phenomenon can be seen in both Figure 10 and the 40.4 and 48.9 Hz traces of Figure 12. In the frequency range.of 38 to 48 Hz, the total pressure perturbation amplitude at the main test station was significantly smaller than that at the upstream station. It appeared as if the perturbation at the main test station was being damped out; unfortunately the tunnel frequency range for this calibration wasn't high enough[4] to confirm this. Perhaps directly related to this damping action was the fact that the phase angle between the pressure perturbation at the two stations and the velocity perturbation was a maximum at the same time that the damping action was taking place. Very similar damping of pressure pulses from an acoustic source in an open-ended duct flow was experimentally investigated by Ingard and Singhal [3]. As was the case in this tunnel, they found that the upstream perturbation amplitude was larger than that downstream.

Another item of interest was the hump in the pressure perturbation wave form occurring from 9 to about 16 Hz. This hump can be seen clearly in the 9 Hz trace of Figure 12.

---

[4]48 to 50 Hz was the maximum attainable frequency for this calibration due to the shutter valve pulley configuration.
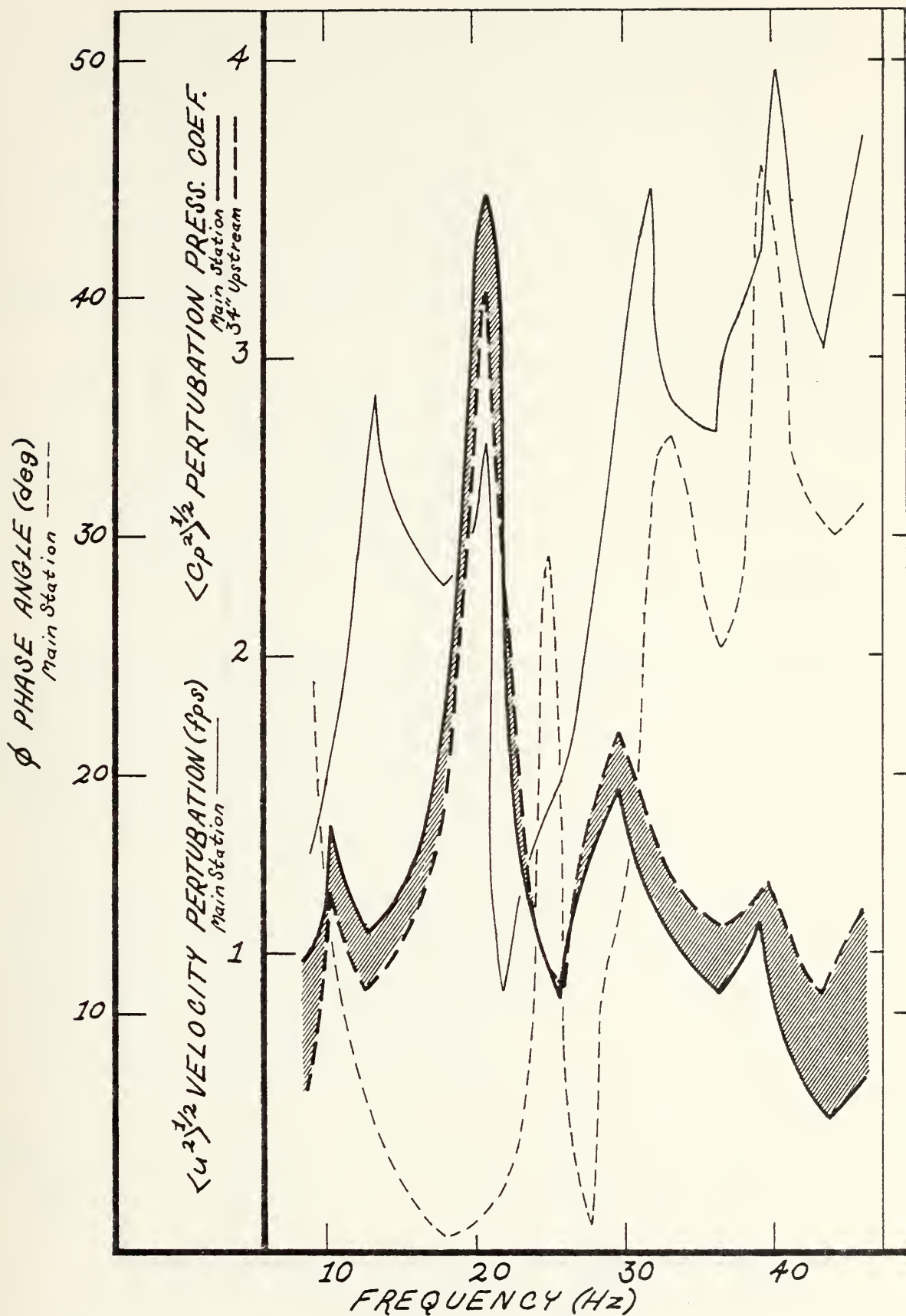
Figure 10. Oscillating Flow Wind Tunnel Frequency Response
Calibration

34
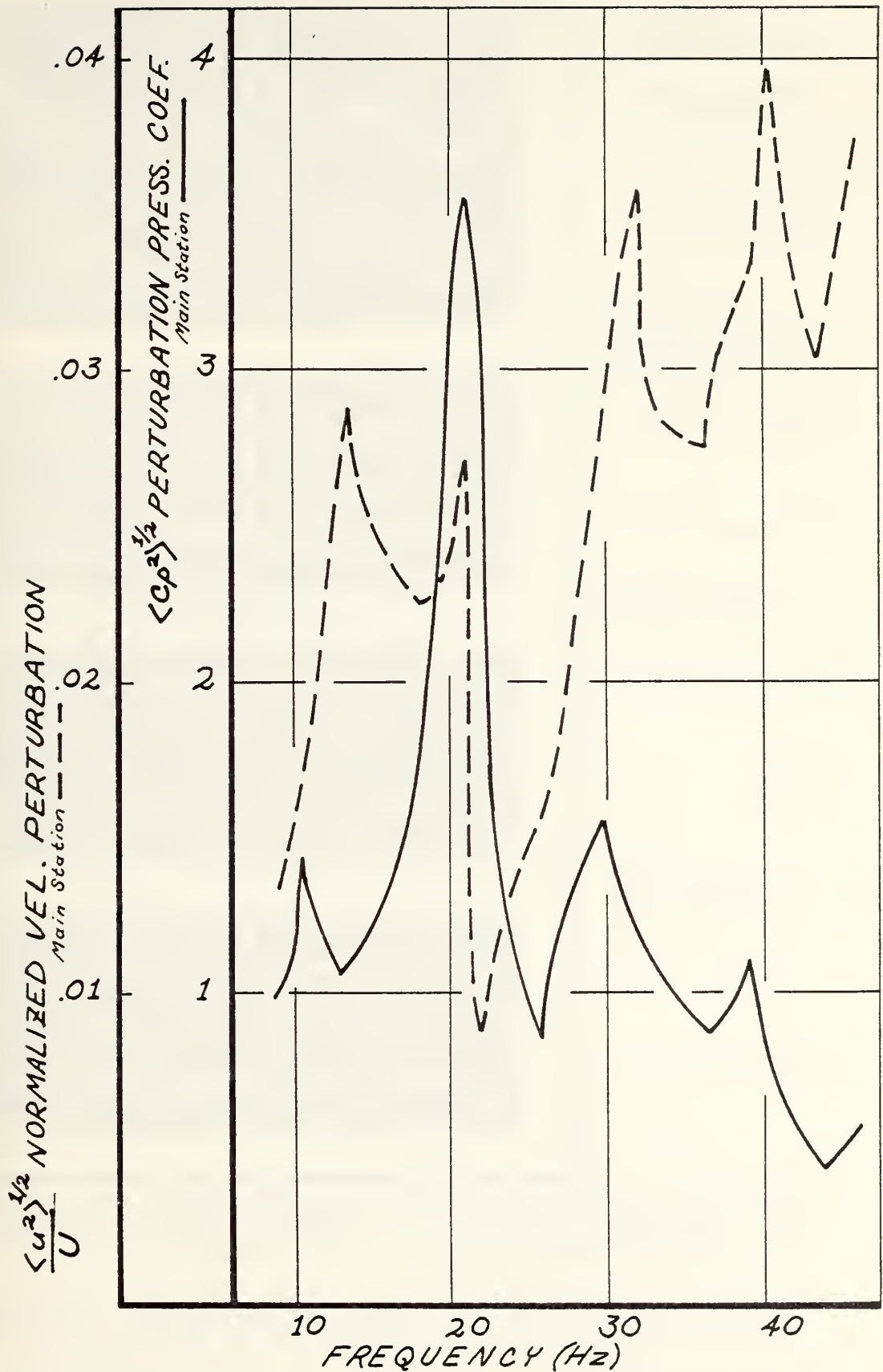
Figure 11. Wind Tunnel RMS C_p and Normalized RMS Velocity
Perturbation Comparison.

35
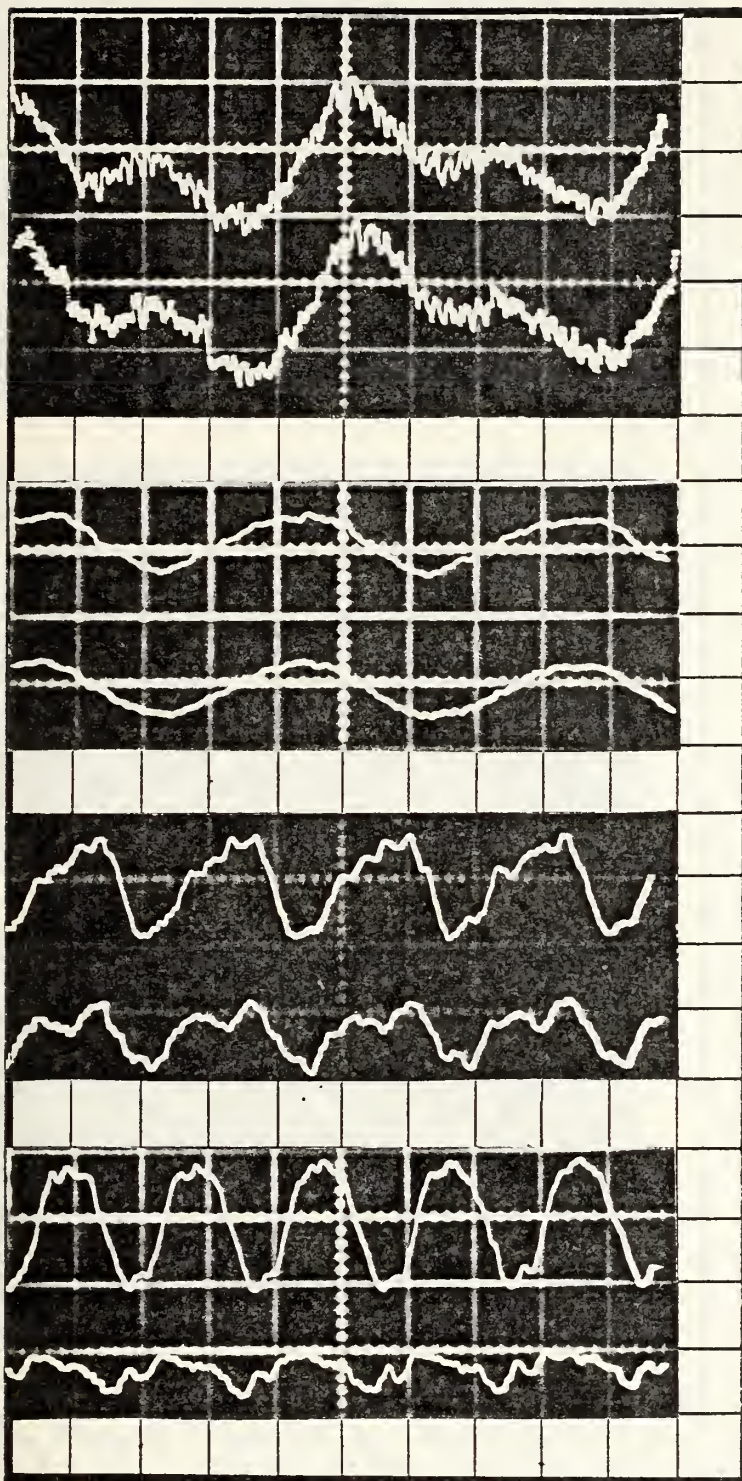
f = 9 Hz
t = 20 msec/division

p = 5.95 psf/div.

p = 5.75 psf/div.

f = 23.2 Hz
t = 10 msec/division

p = 14.61 psf/div.

p = 14.14 psf/div.

f = 40.4 Hz
t = 10 msec/division

p = 14.23 psf/div.

p = 13.78 psf/div.

f = 48.9 Hz
t = 10 msec/division

p = 14.05 psf/div.

p = 13.60 psf/div.

Top Trace: Total Press. 34" Upstream of Wing Station
Bottom : Total Pressure at Wing Station
q = 10 psf, T = 62°F, 3" Blades, t = ↔, p = ↕

Figure 12.   Wind Tunnel Frequency Response Calibration
Oscilloscope Traces
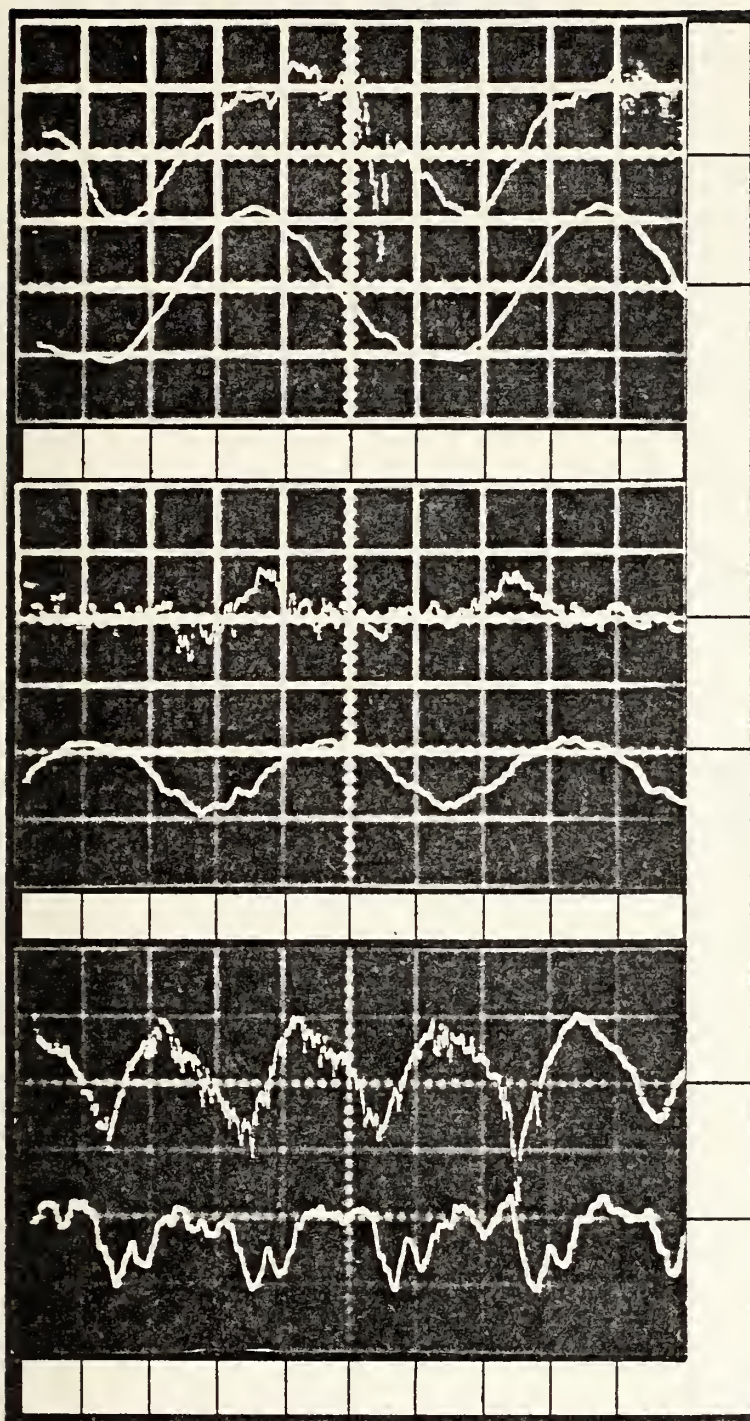
f = 19 Hz
t = 20 msec/div.

V = 18.3 fps/div.

P = 54.8 psf/div.
4" Shutter Blades
_____
3" Shutter Blades
f = 26 Hz
t = 20 msec/div.

V = 4.59 fps/div.

P = 14.6 psf/div.
_____
3" Shutter Blades
f = 46 Hz
t = 10 msec/div.

V = 4.59 fps/div.

P = 5.66 psf/div.

Top Trace : Velocity Perturbation at Wing Station
Bottom : Total Pressure Perturbation, Wing Station
q = 10 psf , T = 64°F, 3 & 4" Blades, t ↔ , P ↕

Figure 13.   Wind Tunnel Frequency Response Calibration
Oscilloscope Traces.
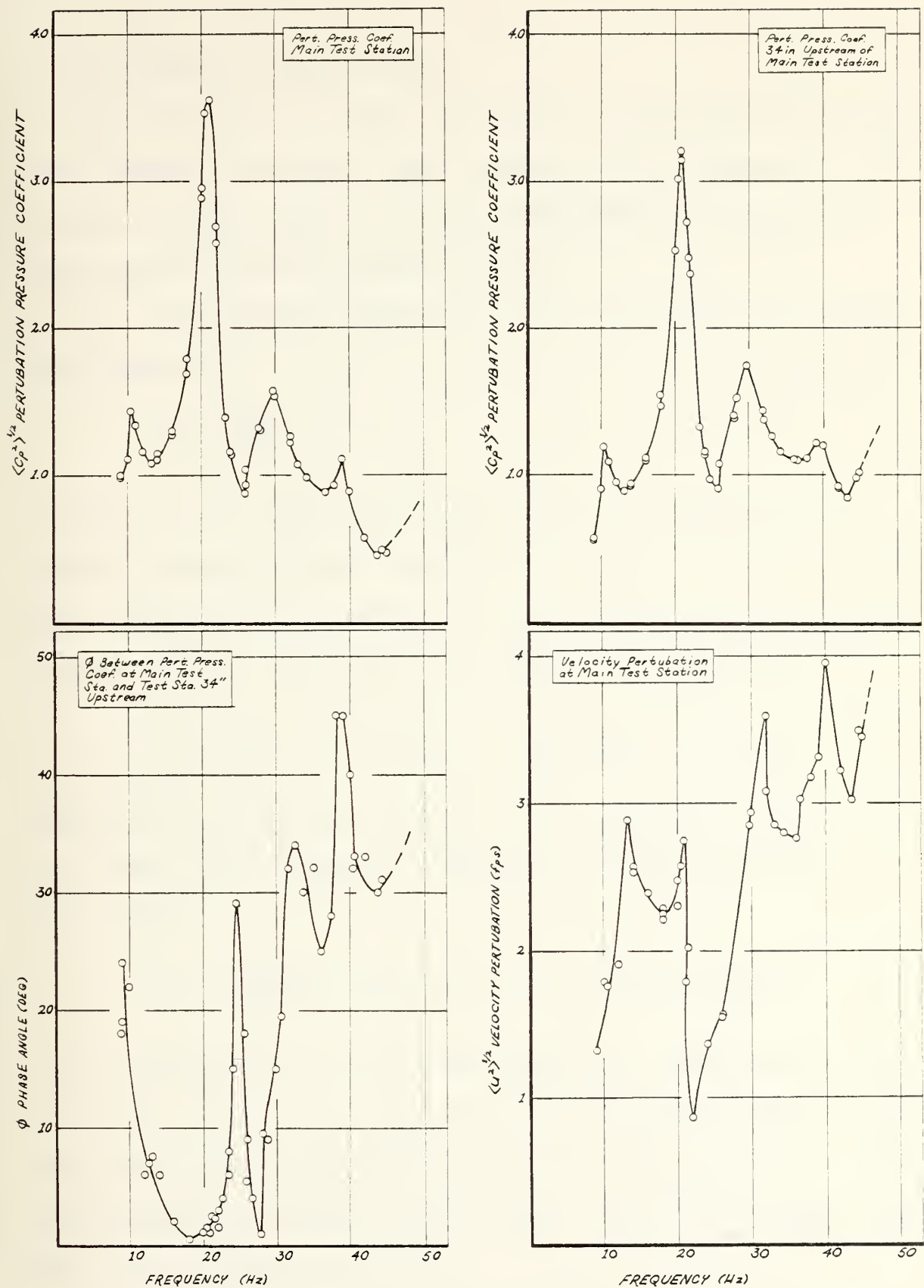
Figure 14. Reduced Data Points for Wind Tunnel Frequency
Response Calibration.

38

B. CCR AIRFOIL SECTION TESTS

The objective of these tests was to quantitatively deter-
mine whether the steady state dC_L/dC_μ would correspond with
the RMS dC_L/dC_μ when a harmonic perturbation in C_μ was
superimposed upon the steady value.

C_μ (the blowing coefficient) was defined in the steady
environment as

$$C_\mu = \frac{\dot{M} U_j}{q S}$$

where $\dot{M}$ was the mass flow rate in the air supply pipe, V_j
was the velocity of the Coanda air out of the airfoil section
slot, q was the test section dynamic pressure, and S was the
airfoil section wing area. For small perturbations

$$\dot{m} = \dot{M}_o (1 + \varepsilon \sin \omega t) \quad , \quad u_j = U_{j_o} (1 + \sigma \sin \omega t)$$

Steady flow calculations support the assumption that $\sigma = \varepsilon$
to a first approximation. Therefore, in the unsteady
environment

$$C_\mu = \frac{\dot{M}_o U_{j_o}}{q S} (1 + 2\varepsilon \sin \omega t) = C_{\mu_o} (1 + 2\varepsilon \sin \omega t)$$

If $\dot{m}$ is measured by a hot wire anemometer installed in the
air supply line (i.e., $e_{HW} = k\dot{m}$), then the DC value of e_{HW}
is a good index of $\dot{M}_o$ and the RMS value of e_{HW} provides the
corresponding unsteady contribution. Thus, $\varepsilon = (e_{HW_{RMS}} / e_{HW_o})$
and $C_{\mu_{RMS}} = 2 (e_{HW_{RMS}} / e_{HW_o}) C_{\mu_o}$

The general oscillating perturbation relation of Total
= Mean + RMS sin(wt + ∅) also holds for oscillating C_L or C_p,

where the mean value should be the same as the steady state value. In Figure 22 the mean and steady state C_p distributions are plotted and it can be seen that they are the same within a few percent. The difference between the steady state and resultant oscillating C_p is due to the RMS or effective value of the superimposed oscillating perturbation.

The steady state C_L vs C_μ for various angles of attack is shown in Figure 16; note the linear ranges for the model installed at -5° and 0° angle of attack, resulting in a dC_L/dC_μ of 29 and 30 respectively. Since the zero lift angle of attack was about -5° and dC_L/dC_μ was linear over the C_μ range that would be examined, -5° angle of attack was chosen for the initial unsteady evaluation. Figure 17 shows the C_p profiles around the trailing edge for various steady C_μ values. Notice that there was an increase in C_p for each increase in C_μ and that as C_μ increased, the rear stagnation point ($C_p = 0$) moved forward down the trailing edge. Figure 18 shows the C_p vs x/c for the same C_μ values; for each C_μ increase, there was a very definite increase in C_p resulting in an increase in C_L. Derived from Figure 17 is Figure 19 showing steady state C_p vs C_μ for $\theta = 40^\circ$. As can be seen, C_p and C_μ appear to vary directly; the RMS values, therefore, should also vary directly. Consequently, if the quasi-steady state assumption were true for the super-imposed oscillating perturbation, then

$$\frac{d\langle C_p^2 \rangle^{1/2}}{d\langle C_\mu^2 \rangle^{1/2}} = \frac{dC_{p_m}}{dC_{\mu_m}} = \frac{dC_{p_0}}{dC_{\mu_0}} \cong 84^{[5]}$$

[5] 84 is the value derived from Figure 19 for this particular CCR airfoil section at -5° angle of attack.

The first oscillating run[6] was made at $C_{\mu_m} = 0.0456$, with a corresponding C_p at $\theta = 40^\circ$ of 4.3. The results around the trailing edge are plotted in Figure 21. For an $\dot{M}_{RMS} = 11.7\%$ of $\dot{M}_m$, the $\%C_{\mu_{RMS}} = 2(\%\dot{M}_{RMS}) = 23.7\%$ of C_{μ_m} or $C_{\mu_{RMS}} = 0.0106$. If the quasi-steady assumption holds, then the $C_{P_{RMS}}$ would be $84(0.0106) = 0.89$. In Figure 21 it can be seen that the $C_{P_{RMS}} = 0.45$. This means that the steady state value has actually been attenuated some 50%. This suggests an attenuation in the dynamic transfer function as shown in Figure 15. A similar attenuation in dynamic transfer function for oscillating jet flaps was reported by Simmons [12].
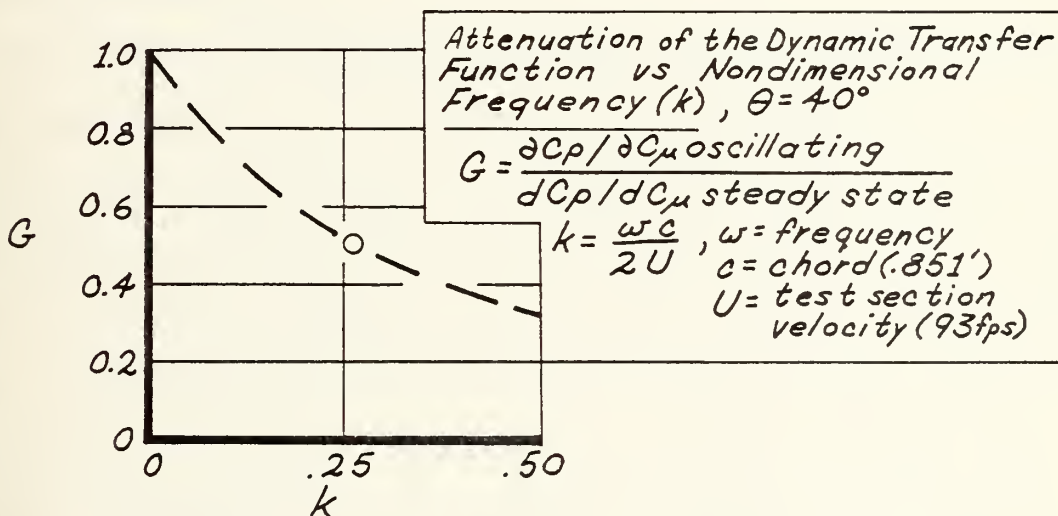
Figure 15. Suggested Attenuation of the Dynamic Transfer Function.

The question then arises, if the $C_{p_{RMS}}$ has attenuated 50% of the steady state value halfway around the trailing edge, how much has it attenuated on the upper and lower airfoil

---

[6]Run 51003.

surfaces? Unfortunately, with the described data acquisition system this case could not be observed due to the tunnel pressure noise level.

Figure 20 shows the midchord upper and lower surface C_p vs C_μ. The upper surface $dC_p/dC_\mu = -17.3$ while that of the lower surface is 6.2. For the first oscillating C_μ run, the maximum C_{pRMS} that could have been generated on the lower surface would have been $C_{pRMS} = 6.2(0.0106) = 0.066$. The RMS C_p noise level was 0.070[7]; therefore, the C_{pRMS} due to blowing oscillation could not have been seen above the noise. This can be seen in the oscilloscope traces of Figures 24 and 25.

The second and third test runs[8] were conducted at rotameter settings of 0.58 and 0.70, corresponding to $C_\mu = 0.0423$ and 0.0630, respectively. For these test runs two things were done which were not done on the first test run. First, prior to each oscillating run a steady run was made to determine the RMS noise levels of the air supply pipe velocity, plenum C_p, and airfoil surface C_p. Second, through very careful adjustment of the plenum air supply line valves, a true C_{pRMS} of 28.4% and 15.9%, respectively, was obtained. The two runs were made at different C_μ values in order to get a trend comparison of oscillating mean and RMS C_μ and C_L versus steady state C_μ and C_L.

_____

[7]RMS C_p noise level based on run 52601 data.

[8]Runs 52601, 52603, 52604, and 52605.

The resulting mean and RMS C_μ versus C_L for the two runs are plotted in Figure 23. Notice that mean C_L/C_μ is the same as the steady value for the first run and within 5% of the steady value for the second. The most noticeable result of these two runs was that the RMS C_μ is less for the higher blowing case, where the rotameter was set at 0.70. This result, however, was not due to airfoil section aerodynamics but rather to the capacity of the air supply compressor. For a given plenum total pressure at high blowing rates, the air compressor used for these tests lacked sufficient capacity to supply enough mass flow to maintain the given plenum total pressure and a high amplitude superimposed perturbation oscillation. This can be seen from the 12.5% reduction in C_{pRMS} for a 0.02 increase in C_μ. It can also be seen visibly in the oscilloscope traces of Figure 25.
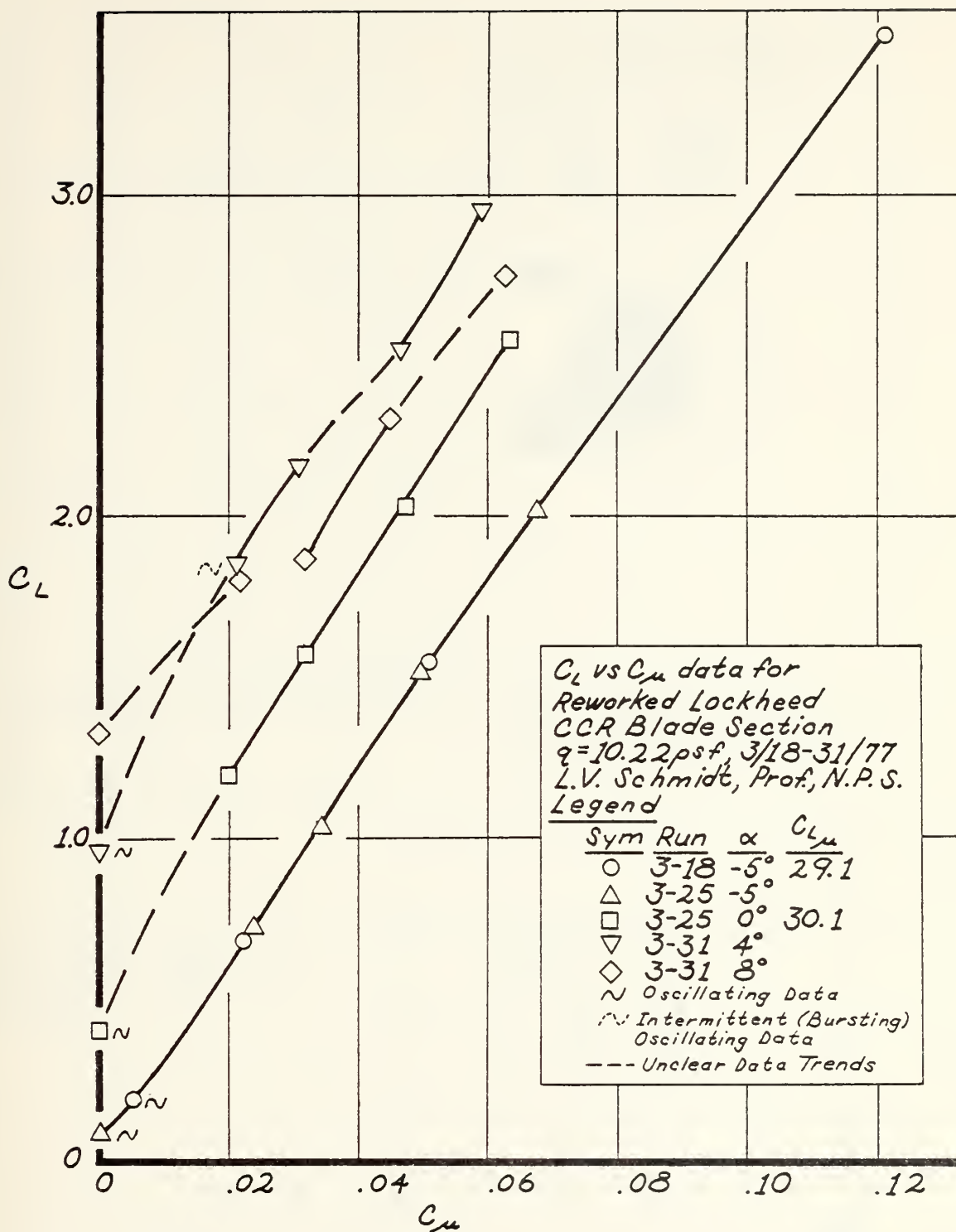
Figure 16. Steady State CCR Airfoil Section C_L vs C_μ
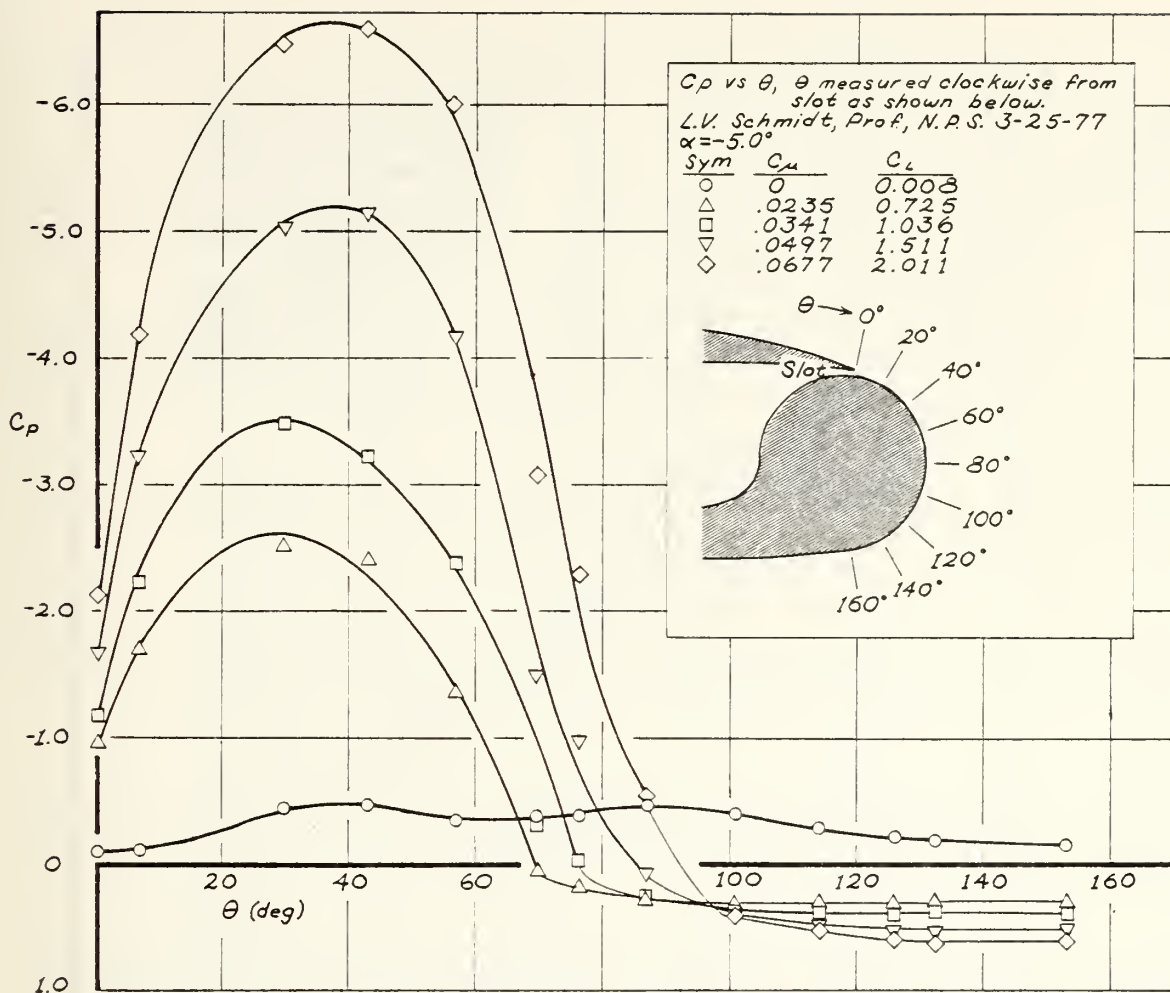
Figure 17. Steady State CCR Trailing Edge C_p Profiles.
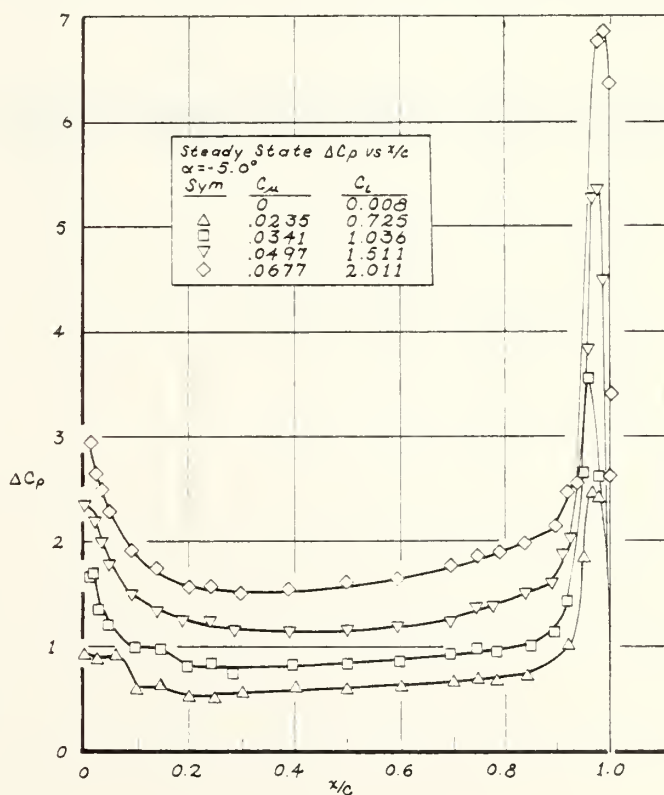
Figure 18. Steady State CCR C_p Distribution Profiles.
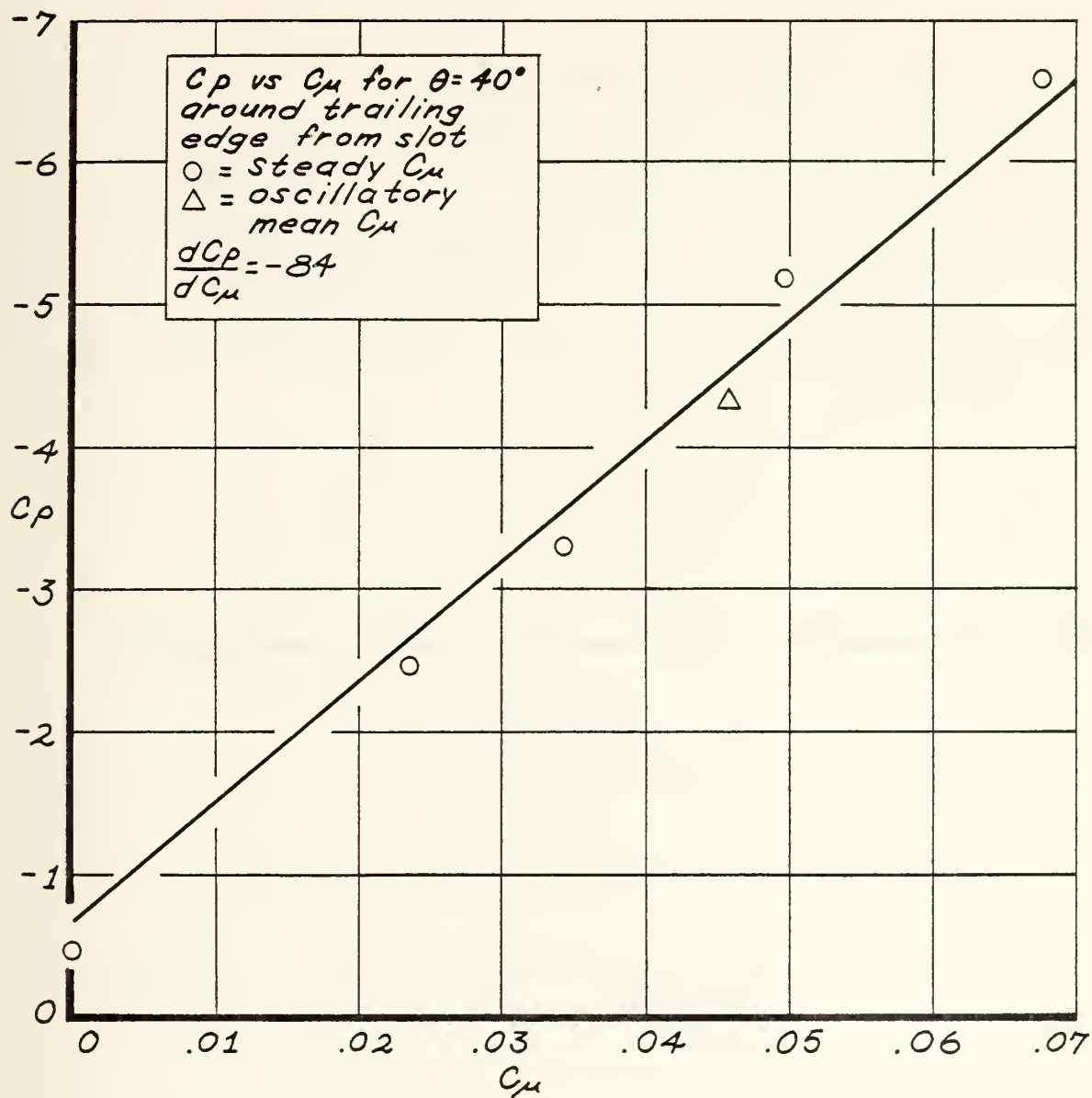
Figure 19. Steady State CCR Trailing Edge dC_p/dC_μ

46
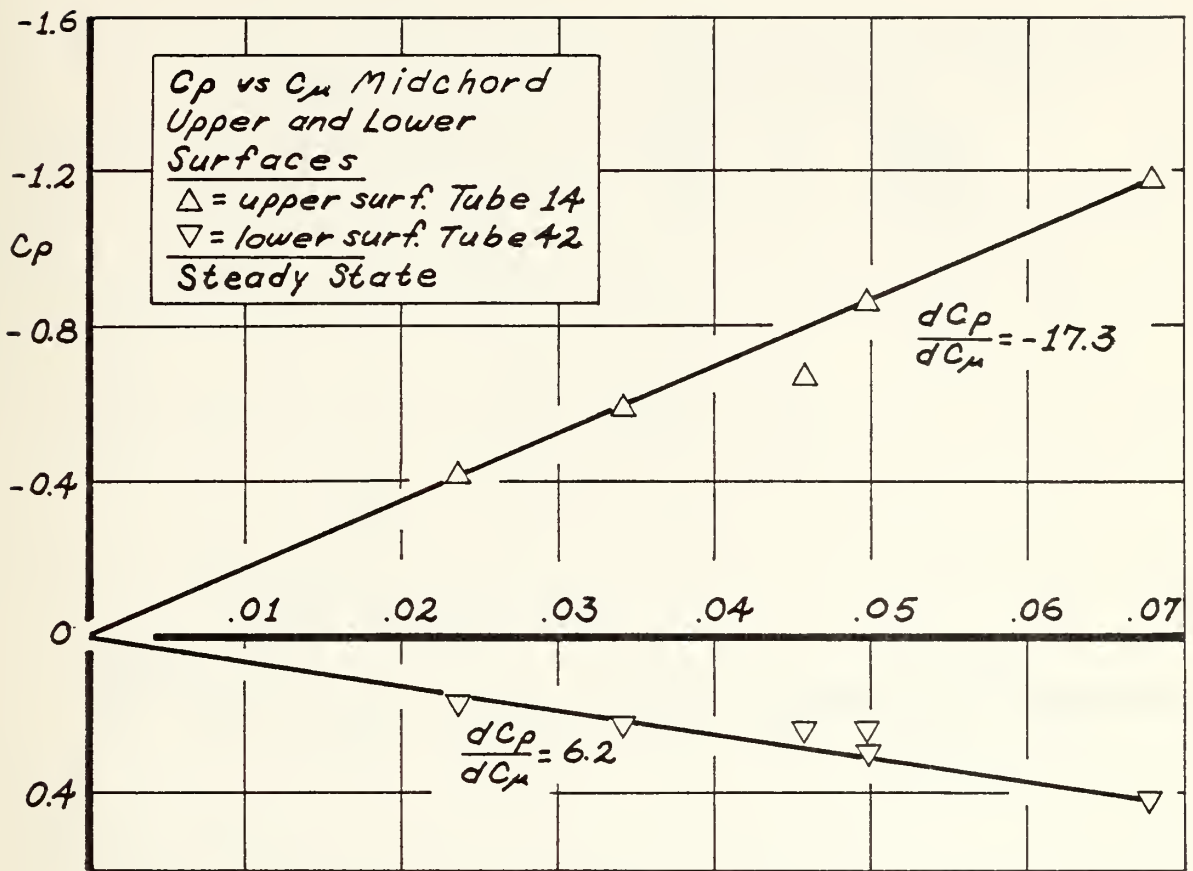
Figure 20. Steady State CCR Upper and Lower Surface
Midchord dC_p/dC_μ
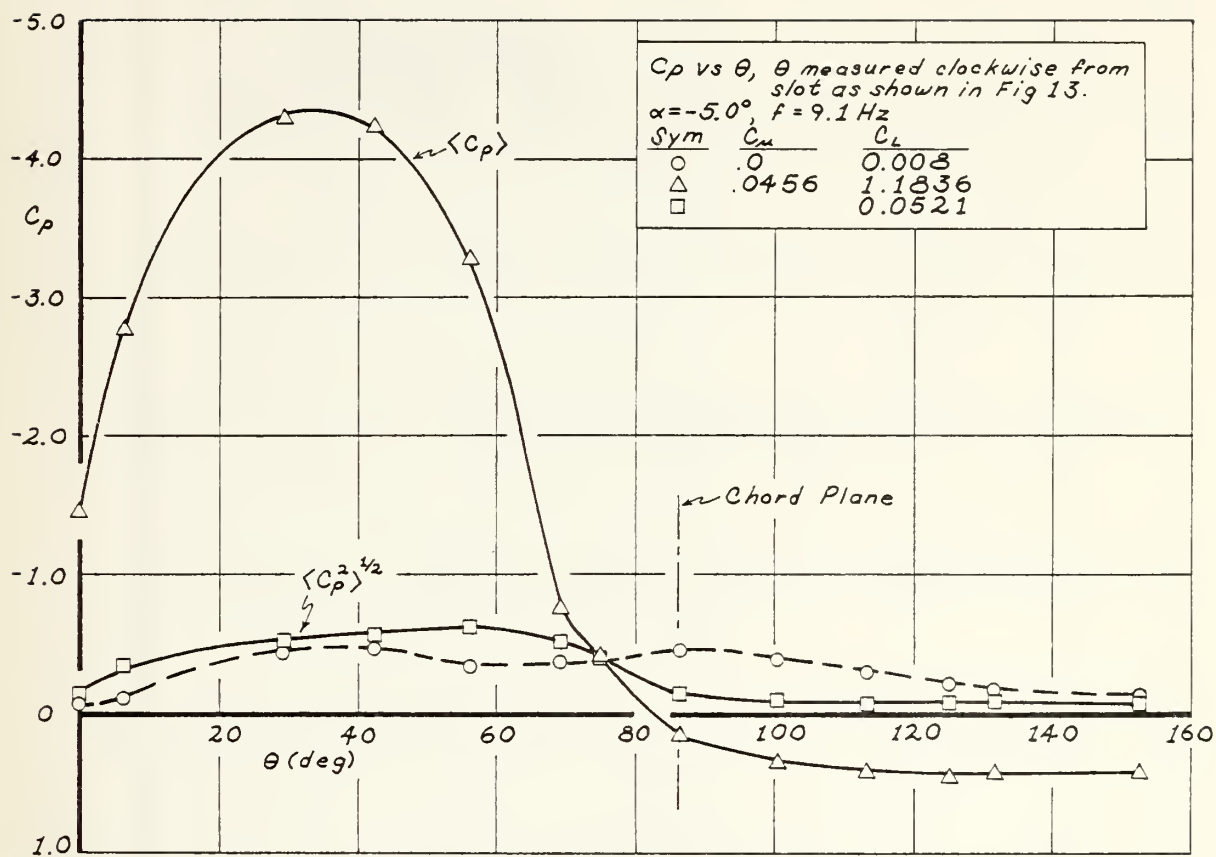
Figure 21. Unsteady CCR Trailing Edge Mean and RMS C_p Profiles.
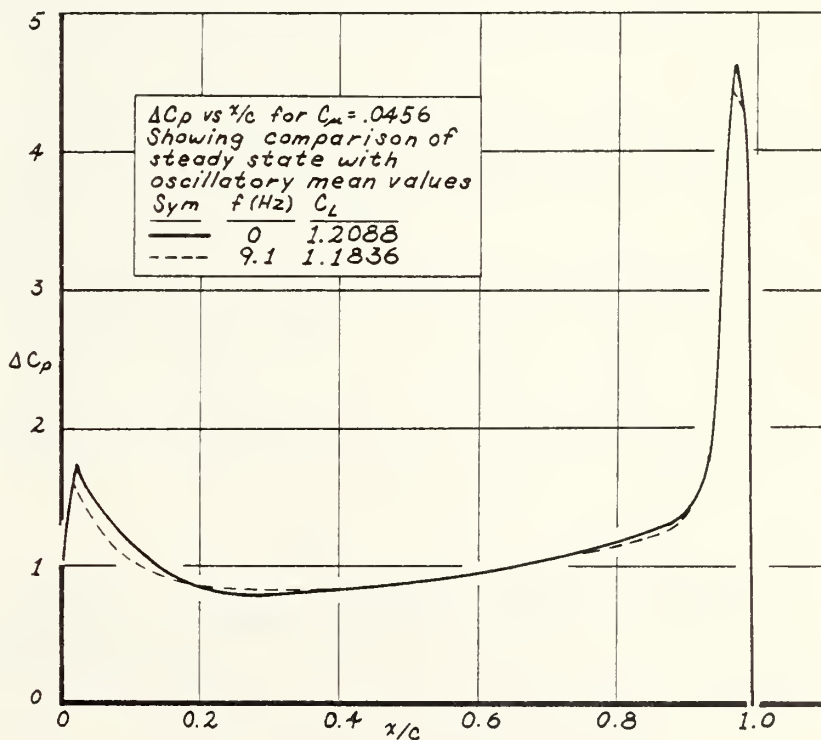
Figure 22. CCR Unsteady Mean and Steady State C_p Distribution Comparison

48
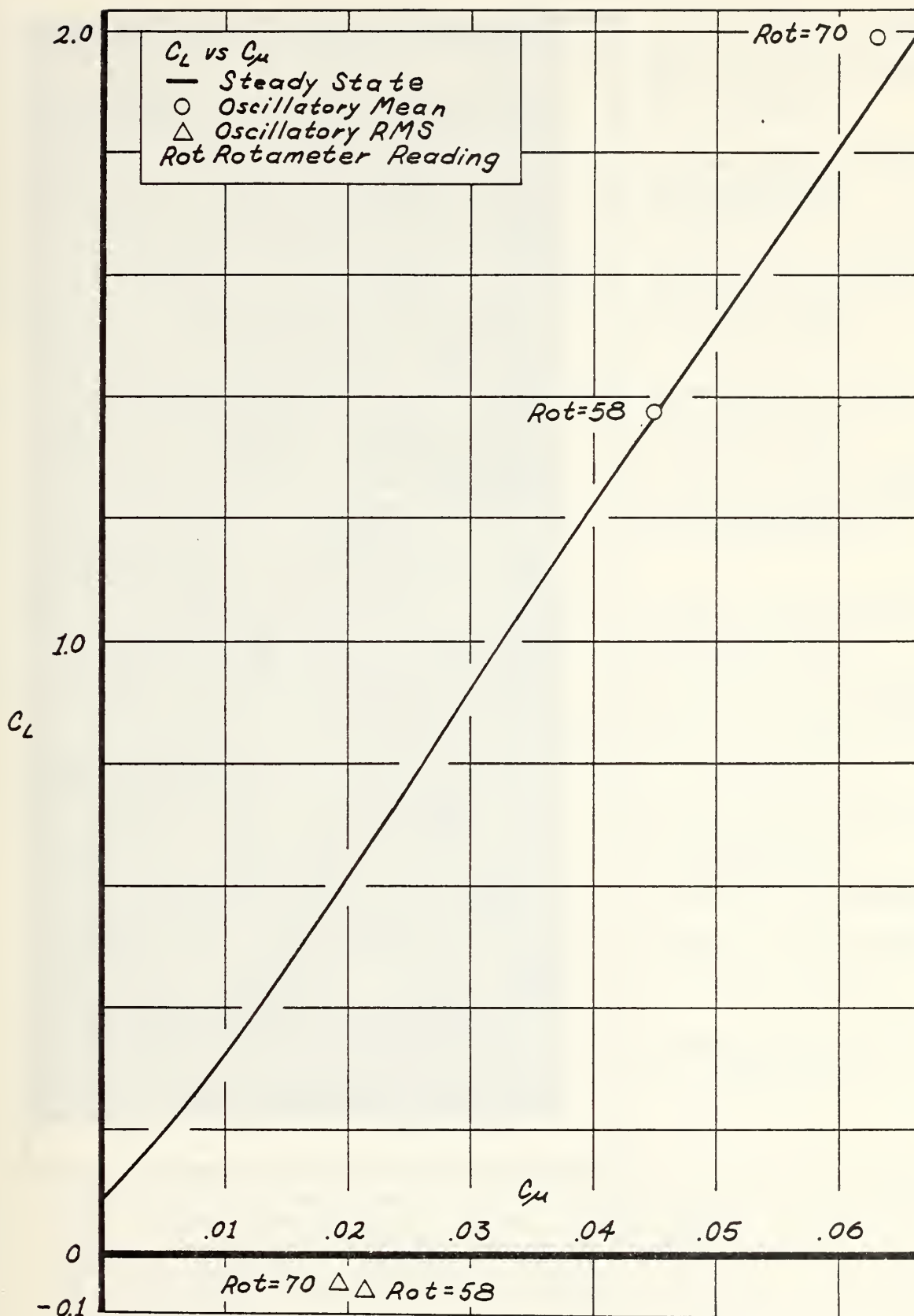
Figure 23. CDR Unsteady Mean - RMS and Steady State
dC_L/dC_μ Comparison

f = 0 Hz, t = 20 msec/div.
Upper Static Press.
P = 1.40 psf/div.

Lower Static Press.
P = 1.48 psf/div.

f = 9.1 Hz, t = 20 msec/div.
Upper Static Press.
P = 2.81 psf/div.

Lower Static Press.
P = 2.96 psf/div.

f = 9.1 Hz, t = 20 msec/div.
Plenum Static Press.
P = 1.48 psf/div.

Lower Static Press.
P = 1.48 psf/div.

f = 9.1 Hz, t = 20 msec/div.
Plenum Static Press.
P = 2.95 psf/div.

Trailing Edge Static Pr.
P = 2.96 psf/div.

f = 9.1 Hz, t = 20 msec/div.
Plenum Static Press.
P = 1.48 psf/div.

Leading Edge Static Pr.
P = 1.48 psf/div.

Oscilloscope Traces of Airfoil Surface Static Pressures
and Airfoil Plenum Cavity Static Pressure
Upper Surface x/c = .4990, Lower Surface x/c = .4998
Leading Edge x/c = .0009, y/c = -.0069
Trailing Edge (behind slot) x/c = .9603, y/c = .0472
q = 10.22 psf

Figure 24. CCR Unsteady Oscilloscope Traces.

50

f = 9 Hz, C_μ = .042
t = 50 msec/divison
Plenum
P = 59 psf/div.

Lower Surface
P = 2.96 psf/div.

f = 9 Hz, C_μ = .063
t = 50 msec/divison
Plenum
P = 59 psf/div.

Lower Surface
P = 2.96 psf/div.
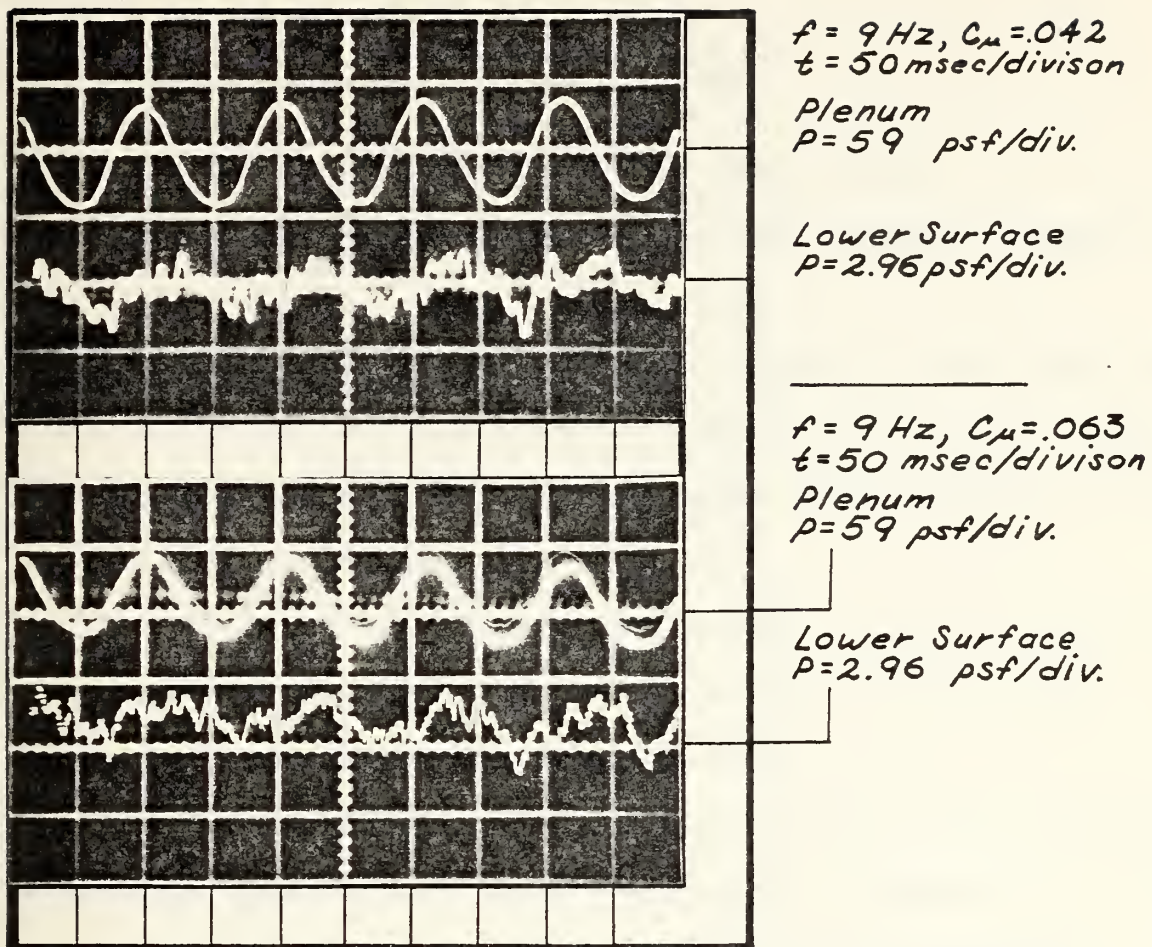
Oscilloscope Traces of Airfoil Plenum Cavity Static Pressure and Lower Surface Static Pressure x/c = .4998 q = 10.22 psf

Figure 25.   CCR Unsteady Oscilloscope Traces.

51

IV. CONCLUSIONS

A. WIND TUNNEL FREQUENCY RESPONSE CALIBRATION

The results discussed point out the following essential facts:

1. RMS C_p perturbations are an order of magnitude greater than the normalized RMS velocity perturbation, which suggests that the tunnel flow is governed by Euler's equation in conjunction with wave mechanics.

2. The wind tunnel frequency response clearly exhibits at least four resonant frequencies between 9 and 48 Hz. The primary resonant frequency was about 21 Hz.

3. The oscillating pressure perturbation was most nearly sinusoidal immediately about the resonant frequencies. The best sinusoidal wave form was observed in the frequency range of about 19 to 24 Hz.

4. The oscillating pressure perturbation at the main test station was being damped out from 38 to 48 Hz. The highest frequency which could be obtained in this calibration was 48 Hz.

B. CCR AIRFOIL SECTION TESTS

The results discussed point out the following essential facts:

1. The dC_p/dC_μ decreases as the oscillating blowing frequency increases. This suggests an attenuation in the dynamic transfer function.

2. The RMS C_p noise level in the tunnel is significant ($\langle c_p^2 \rangle^{\frac{1}{2}}$ = 0.07). In order to operate at a signal-to-noise ratio of 10 or greater for representative operational unsteady C_μ values, the tunnel pressure noise or turbulence level must be reduced.

3. The plenum air supply compressor used for these tests lacked sufficient capacity to maintain a high amplitude super-imposed perturbation over a wide range of C_μ values.

Calibration Curves and Airfoil Data
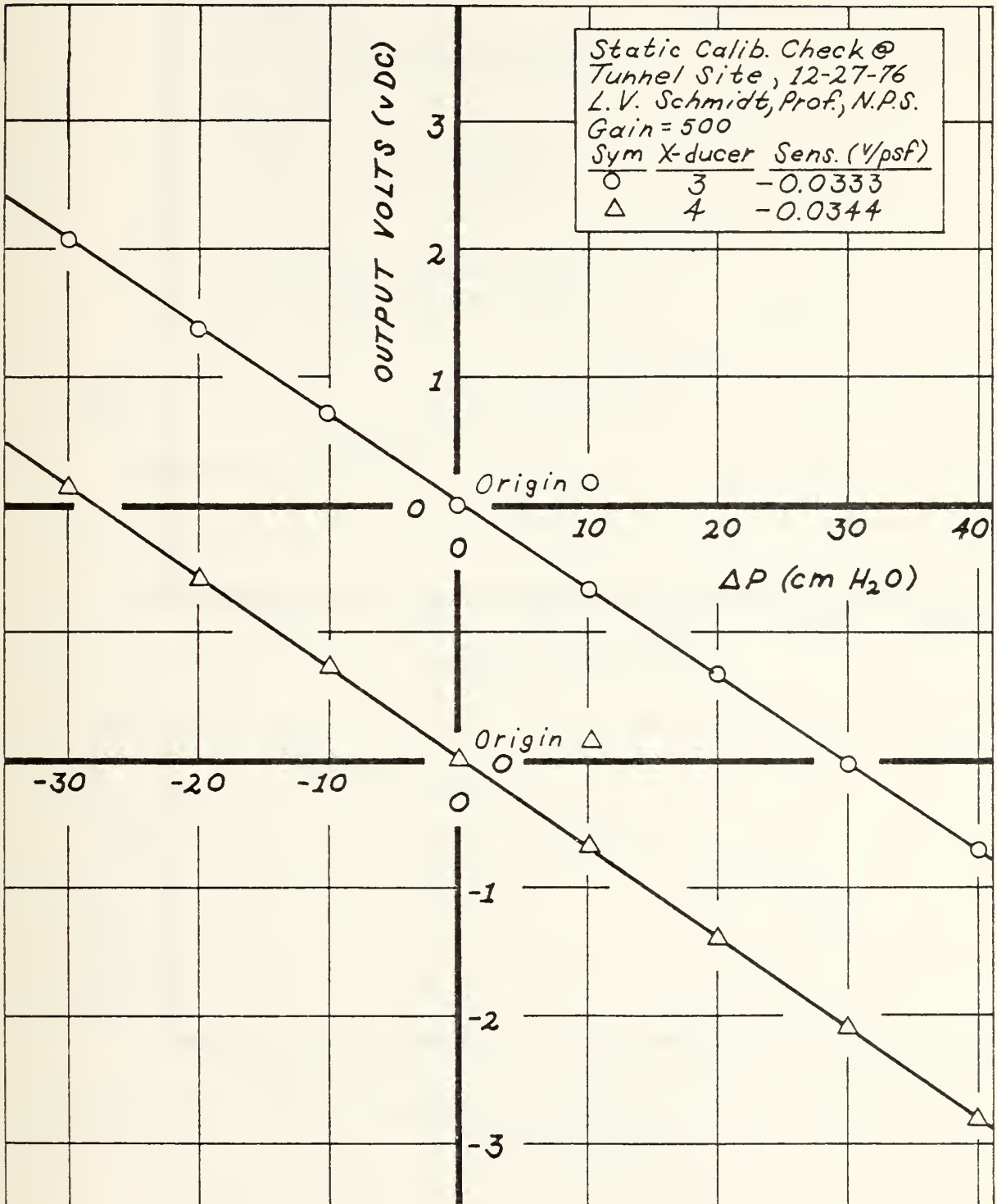
Figure 26. Tunnel Frequency Response Static Transducer
Calibration.

54
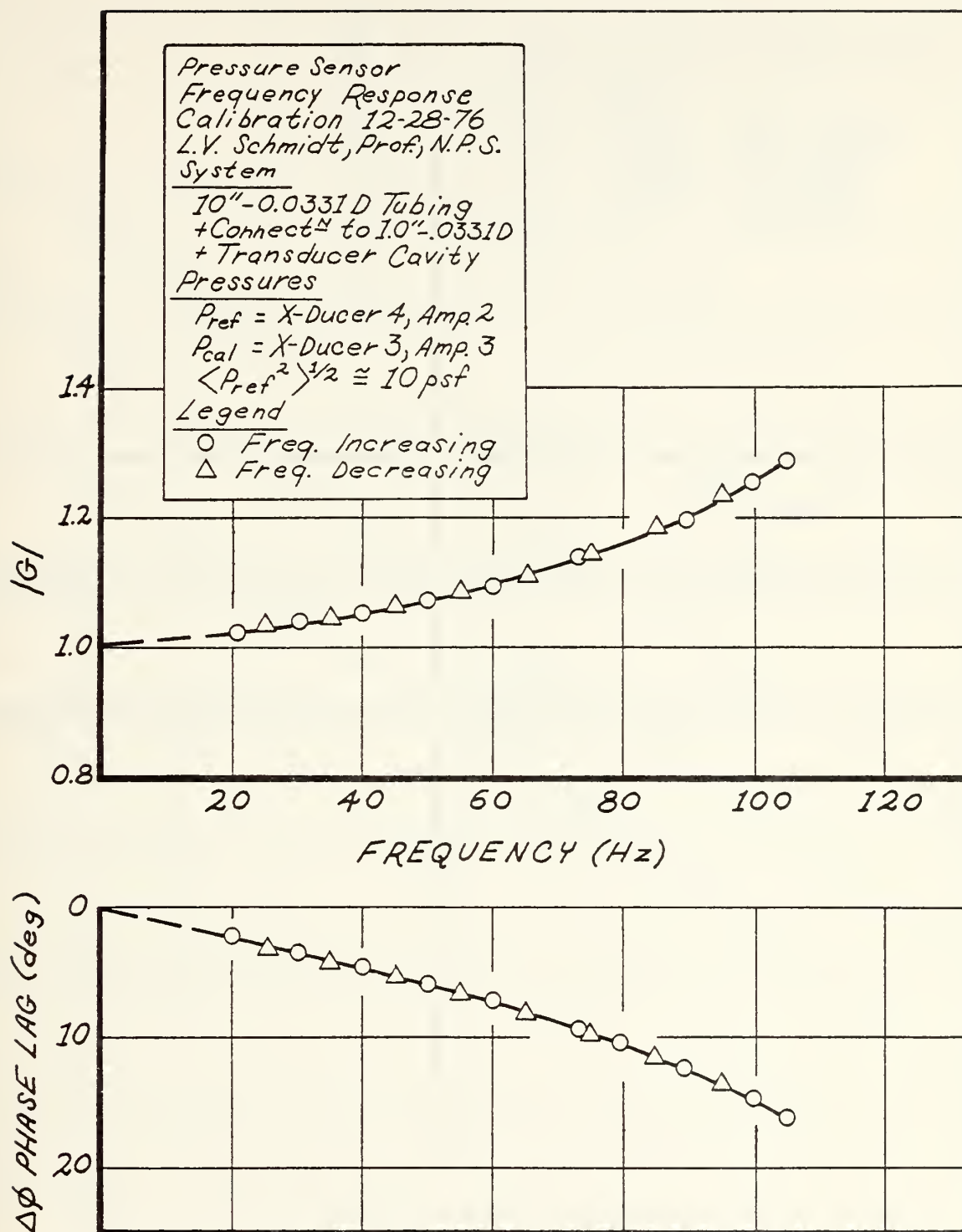
Figure 27. Tunnel Frequency Response Dynamic Transducer Calibration.
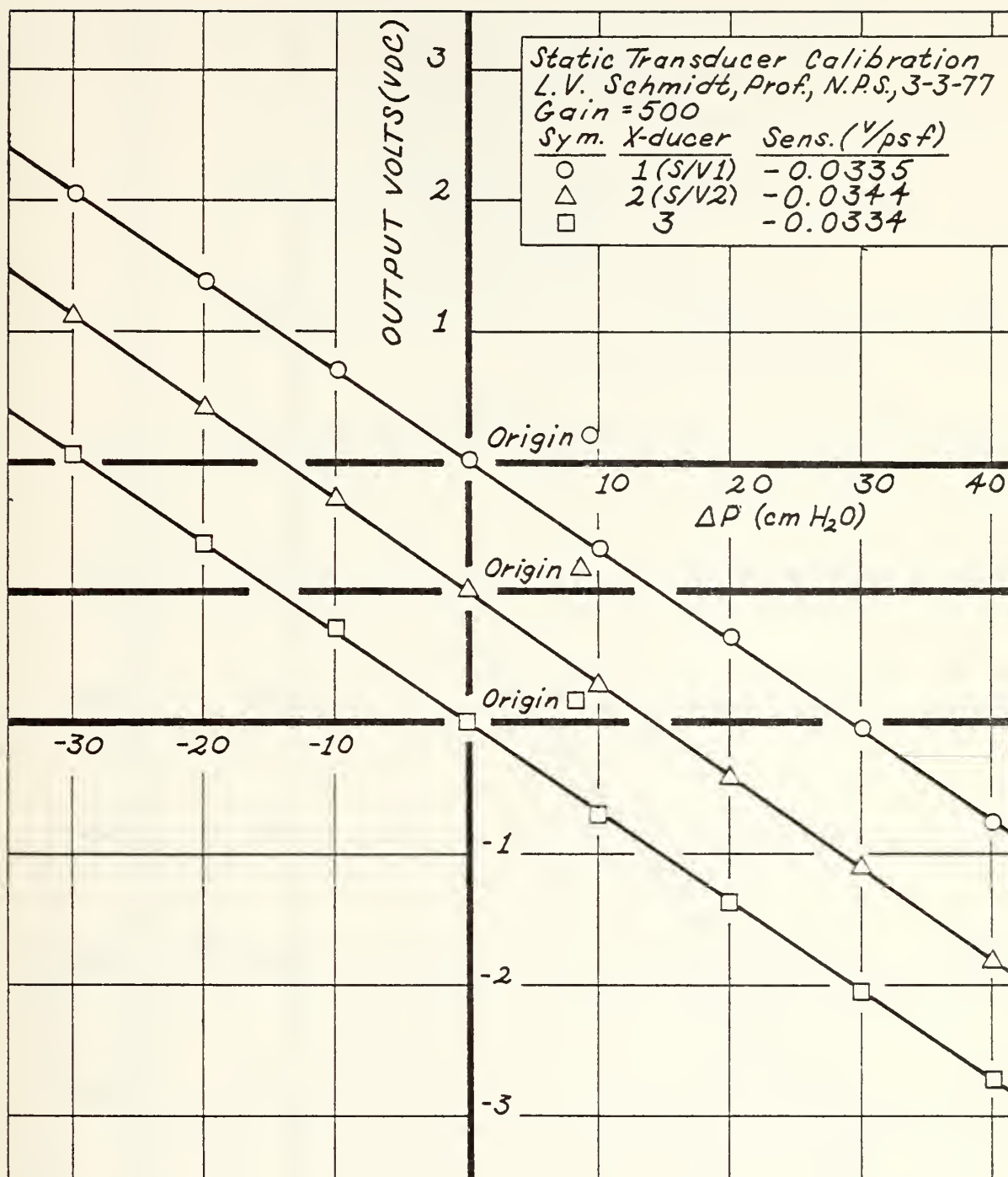
Figure 28. CCR Tests Static Transducer Calibration.
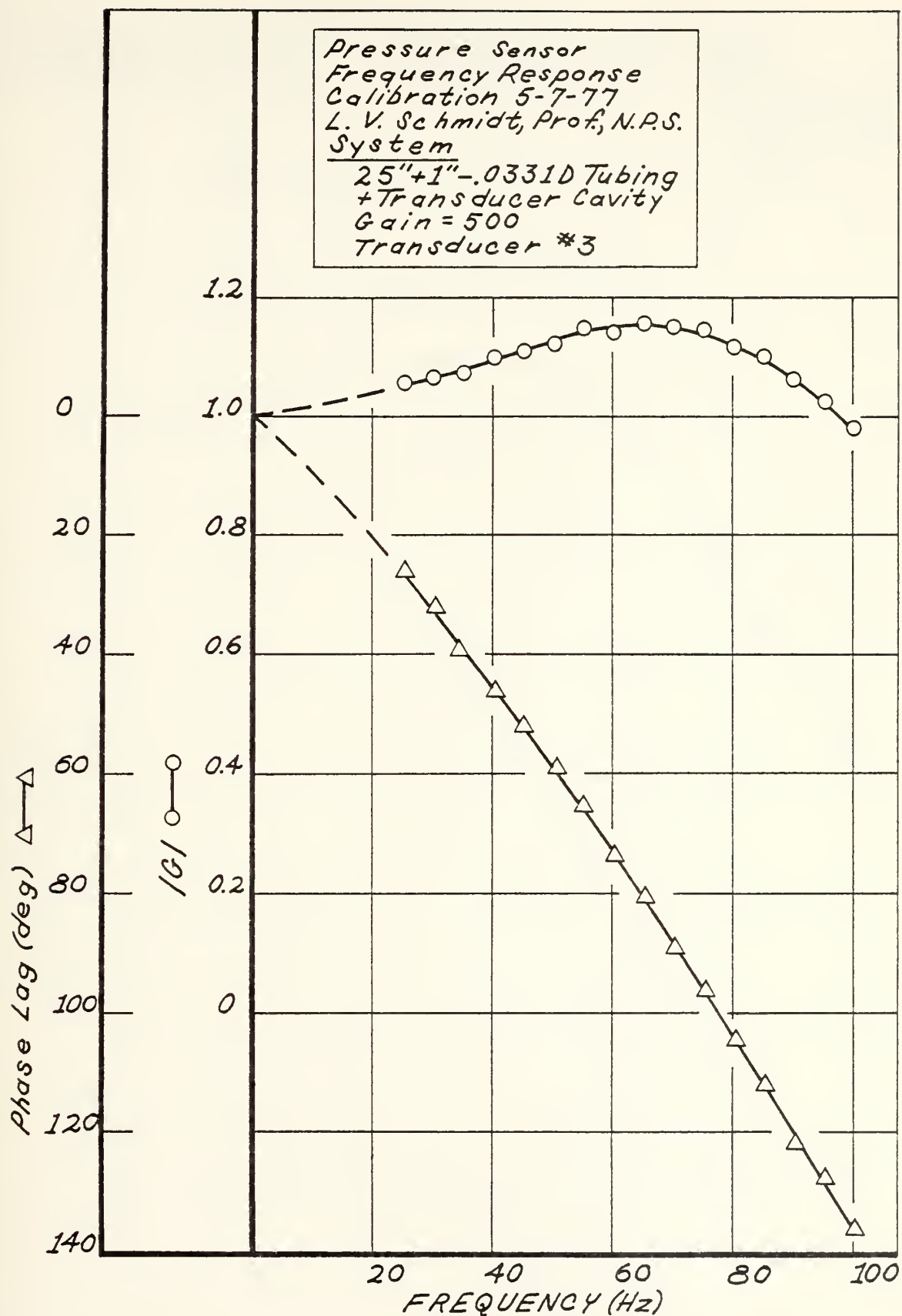
Figure 29.   CCR Tests Dynamic Transducer Calibration.
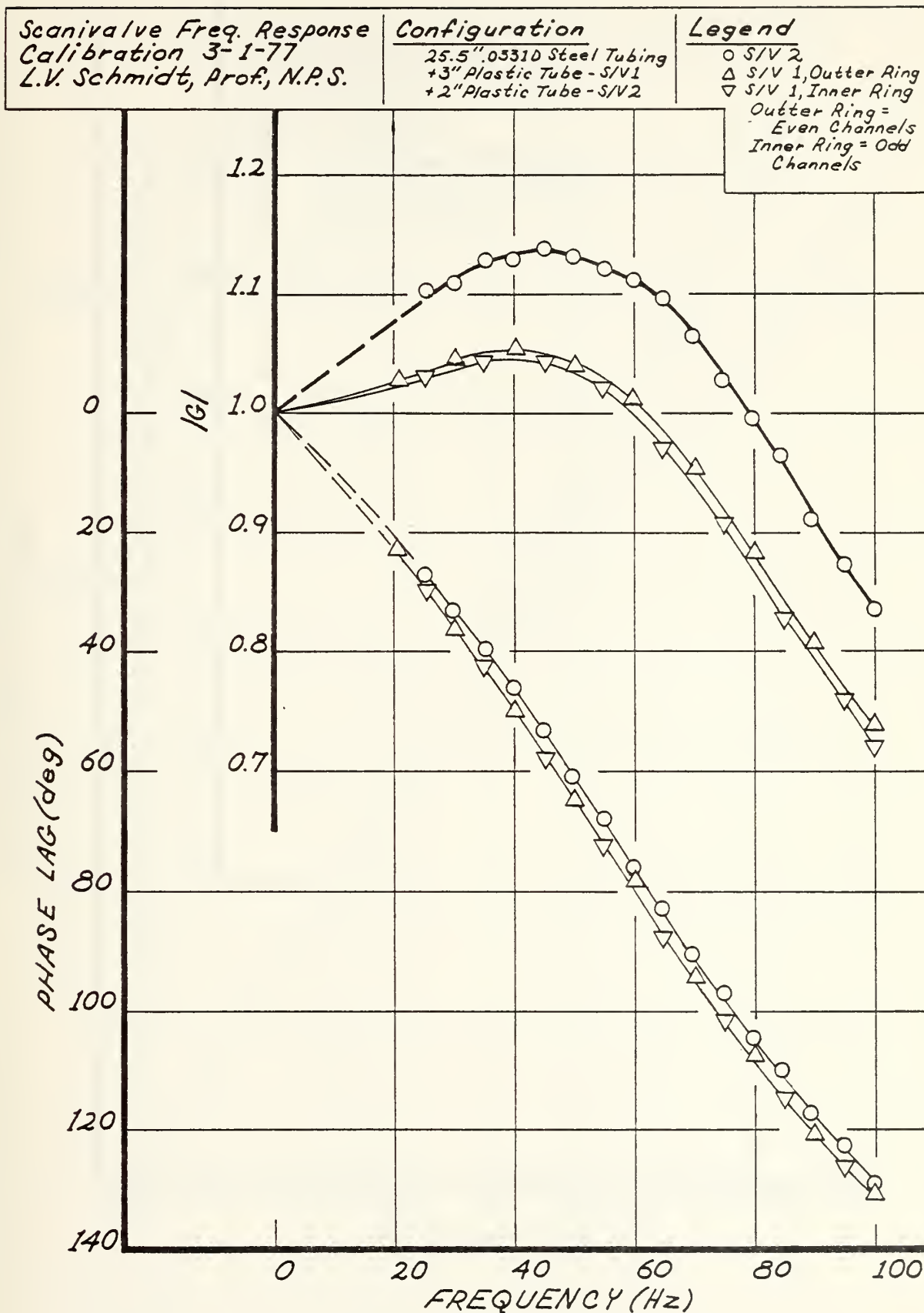
Figure 30. CCR Tests Dynamic Transducer Calibration.
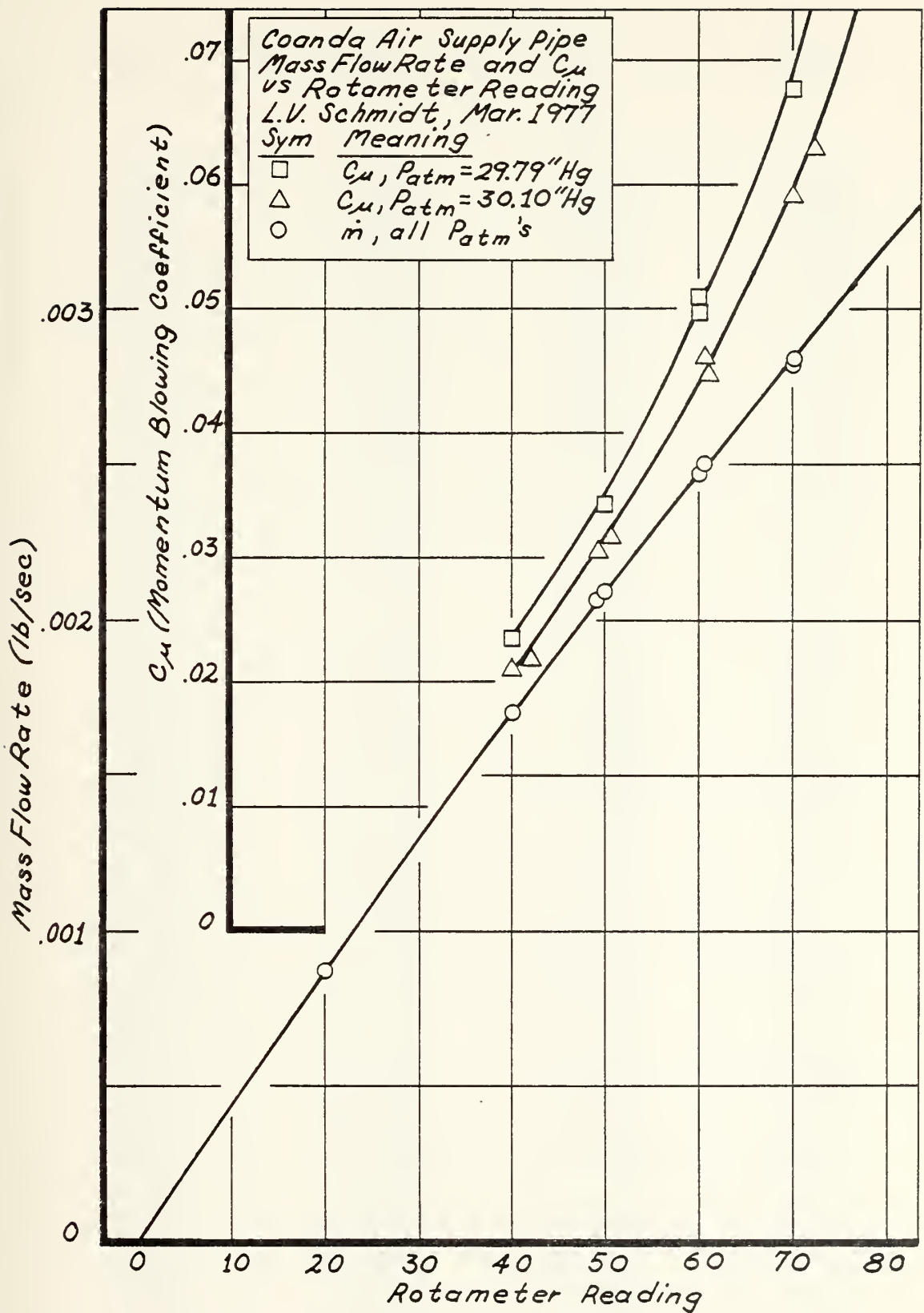
Figure 31. CCR Tests Rotameter Calibration.

59

Table I. CCR Airfoil and Pressure Tap Coordinates

Tap No.	x (in.)	x/c	y (in.)	y/c
1	0.0	0.0	0.0	0.0
2	0.012	0.0012	0.084	0.0083
3	0.060	0.0059	0.173	0.0170
4	0.119	0.0117	0.247	0.0242
5	0.213	0.0209	0.335	0.0328
6	0.314	0.0308	0.406	0.0398
7	0.517	0.0507	0.528	0.0517
8	0.949	0.0930	0.728	0.0713
9	1.431	0.1402	0.897	0.0879
10	1.929	0.1890	1.038	0.1017
11	2.433	0.2384	1.149	0.1126
12	2.848	0.2791	1.224	0.1199
13	3.954	0.3874	1.357	0.1329
14	5.093	0.4990	1.396	0.1368
15	6.098	0.5975	1.347	0.1320
16	7.130	0.6986	1.226	0.1201
17	7.635	0.7481	1.134	0.1111
18	8.021	0.7859	1.053	0.1031
19	8.670	0.8495	0.881	0.0863
20	9.191	0.9005	0.713	0.0698
21	9.400	0.9210	0.635	0.0622
22	9.598	0.9404	0.560	0.0549
23	9.801	0.9603	0.482	0.0472
24	9.949	0.9748	0.410	0.0402
25	10.053	0.9850	0.339	0.0332
26	10.135	0.9930	0.245	0.0240
27	10.182	0.9976	0.145	0.0142
28	10.193	0.9987	0.090	0.0088
29	10.206	1.0000	0.0	0.0
30	10.194	0.9988	-0.118	-0.0115
31	10.152	0.9947	-0.223	-0.0219
32	10.109	0.9905	-0.307	-0.0301
33	10.040	0.9837	-0.349	-0.0342
34	9.919	0.9719	-0.448	-0.0439
35	9.769	0.9572	-0.524	-0.0514
36	9.590	0.9396	-0.580	-0.0569
37	8.552	0.8379	-0.695	-0.0681
38	7.946	0.7786	-0.740	-0.0725
39	7.562	0.7409	-0.758	-0.0742
40	7.042	0.6900	-0.775	-0.0759
41	6.023	0.5901	-0.786	-0.0770
42	5.101	0.4998	-0.788	-0.0772
43	4.005	0.3924	-0.772	-0.0756
44	2.885	0.2827	-0.736	-0.0721
45	2.480	0.2430	-0.708	-0.06944
46	1.969	0.1929	-0.658	-0.0645
47	1.471	0.1441	-0.594	-0.0582
48	0.953	0.0934	-0.517	-0.0506
49	0.515	0.0505	-0.416	-0.0408

Table I (cont'd)

Tap No.	x (in.)	x/c	y (in.)	y/c
50	0.345	0.0338	-0.349	-0.0342
51	0.229	0.0224	-0.285	-0.0280
52	0.119	0.0117	-0.214	-0.0210
53	0.053	0.0052	-0.145	-0.0142
54	0.009	0.0009	-0.070	-0.0069

Uppr. Surf. spcl. tubes

55	5.108	0.5004	6.0 inches		Distance
56	5.093	0.4990	9.0 "		Stb'd
57	5.095	0.4992	10.5 "		from
58	7.631	0.7477	6.0 "		center
59	7.631	0.7477	9.0 "		

All tubes are 25.5 inches in length, 0.033 in. I.D., and
0.050 O.D. Tubes have been renumbered from identification
existing at Nov. '76 when model was removed from tunnel for
t.e. slot rework. Two new tubes have been installed.
Note, the slot is located at x = 9.748 in., x/c = 0.9551 ....

Table II. Scanivalve Channel Log

S/V 1 (48 channel)   S/V 2 (24 channel)

chnl	tap loc.	chnl	tap loc.	chnl	tap loc.	chnl	tap loc.	chnl	tap loc.
0(48)	atm	18	22	36	54	0(24)	atm	18	32
1	P_s	19	37	37	55	1	P_s	19	33
2	P_t	20	38	38	56	2	P_t	20	34
3	7	21	39	39	57	3	1	21	35
4	9	22	40	40	58	4	2	22	36
5	11	23	41	41	59	5	3	23	atm
6	17	24	42	42-47	plenum	6	4		
7	19	25	43			7	5		
8	20	26	44			8	6		
9	21	27	45			9	8		
10	23	28	46			10	10		
11	24	29	47			11	12		
12	25	30	48			12	13		
13	26	31	49			13	14		
14	27	32	50			14	15		
15	28	33	51			15	16		
16	29	34	52			16	18		
17	30	35	53			17	31		

EXPERIMENTAL DATA

Table III. Experimental Data, Tunnel Frequency Response

Run 21401[1]
3 in. blades, q=10 psf

f (Hz)	P_t 34" upstrm x-ducer 4		P_t wingsta x-ducer 3		Velocity wingsta		Ø (deg)	Notes
	VDC	VRMS	VDC	VRMS	VDC	VRMS		
0	0	.00215	0	.00194	-.002	.00069		q=0
0	.012	.0028	-.015	.003				
52		.45		.157			135	
9		.202		.235		.0145	19	
10		.317		.369		.0195	8	
10.4		.417		.482		.0190	6	
12.0		.334		.392		.0208	6	
13.1		.311		.365		.031	7.5	
14		.328		.372		.028	9.5	
16		.386		.432		.026	8.0	
18		.52		.575		.0245	8.0	
20		.89		.98		.025	5.5	
20.9		1.13		1.21		.0195	2.5	
22		.878		.920		.0095	1.5	
24		.405		.398		.015	.5	
25.8		.323		.300		.0168	5.5	
28		.495		.452		.0205	9.5	
29.7		.625		.538		.032	2.5	
32		.495		.422		.0335	0	
34.2		.416		.340		.0305	1.0	
36.6		.397		.308		.033	8	
38		.403		.323		.0345	45	
40		.437		.312		.043	40	
42		.340		.20		.035	29	
43.6		.310		.160		.0330	40	
44.4		.362		.173		.038	28	
0	.011	.024	-.120	.024	.920	.0055		
0	.005		-.127		-.001			q=0

Run 21101

3 in. blades, q=10 psf

0	0	.0023	0	.00345	.002	.00065		q=0
0	.005	.030	.005	.0027	.945	.005		
9		.24		.19		.027	18	
11		.465		.37		.042		
14		.40		.32		.0275	6	
16		.455		.38		.029	2	
18		.63		.53		.024	1	
22		.91		.81		.0185	3	

[1]Run number: 1st digit = month, 2nd & 3rd digits = day, last digit = run of that day.

Table III. (cont'd)

Run 21101 (cont'd)

f (Hz)	P_t 34" upstrm x-ducer 4 VDC	VRMS	P_t wingsta x-ducer 3 VDC	VRMS	Velocity wingsta VDC	VRMS	∅ (deg)	Notes
20.8		1.25		1.075		.030	1	
24		.415		.4		.015	15	
26		.37		.37		.020	9	
27.8		.47		.485		.020	1	
29.8		.545		.60		.031	15	
31.8		.45		.50		.0385	32	
33		.384		.44		.031	30.5	
36		.375		.387		.030	25	
39		.40		.43		.036	45.5	
42		.205		.327		.030	33	
43.6		.167		.30		.031	30	
44.8		.17		.36		.0375	33	
0	.005	.025	−.052	.025	.950	.010		
0	−.001		0.055		.013			q=0

Run 20901
3 in. blades, q=10 psf

0	0	.0045	0	.0054	0	.0063		q=0
0	.008	.005	−.025	.007	.945	.007		
10		.25		.194		.028	22	
12		.47		.392		.042		
18		.685		.58		.025	10	
16		.437		.362		.023	10	
19.8		1.04		.89		.027	10	
20.4		1.22		1.03		.028	1.4	
21.5		.106		.93		.022	2.2	
23.3		.493		.455		.015	8	
24.6		.342		.335		.016	29	
26.6		.352		.355		.015	4	
28.8		.487		.527		.027	9	
30.6		.433		.484		.029	19.5	
32.5		.343		.388		.028	34	
35		.275		.324		.0265	31	
37.5		.285		.345		.029	28	
40.2		.248		.355		.034	32	
44.1		.15		.284		.029	31	
47.2		.139		.384		.047	50	
48.9		.131		.427		.056	63	
40.4		.226		.322		.032	33	
23.2		.440		.406		.014	6.5	
25.6							18	
22.3		.605		.540		.012	4	
18.1		.658		.562		.022	1	
9		,2		.156		.025	24	
12.4		.248		.198		.028	7	
16		.306		.254		.019	2	
0		.036		.033		.005		
0	.001	.0021	−.117	.0019		.0009		q=0

63

Table III. (cont'd)

Run 20402
3 in. blades, q=10 psf

f (Hz)	P_t 34" upstrm x-ducer 4 VDC	VRMS	P_t wingsta x-ducer 3 VDC	VRMS	Velocity wingsta VDC	VRMS	Ø (deg)	Notes
0	.002	.0021	-.001	.00195	.002	.0048		q=0
0	.005	.03	.350	.03	.968	.005		
8		.24		.24		.03	68	
16		.43		.415		.026	64	
20		1.2		1.18		.27		
26		.33		.32		.017	63	
31		.42		.41		.033		
40		.3		.285		.03		
45		.150		.153		.031		
50		.142		.166		.06		
46		.137		.147		.038		
	-.002	.002	-.0083	.0019	.002	.00046		q=0

Run 20401
4 in. blades, q=10 psf

0	o	.0024	0	.0037	.010	.0013		q=0
0	.007	.03	.352	.03	.95	.0065		

Note: Tunnel vibration level too high. 4 in. blades replaced with 3 in. blades.

Run 12801
4 in. blades, q=10 psf

	P_S wingsta x=ducer 4 VDC	VRMS						
0	-.013	.002	.000	.002	.007	.001		q=0
0	-.360	.030	-.005	.040	-.924	.020		
4	-.225	.310	-.005	.310	-.789	.125		
12.5	-.201	.455	.010	.465	-.795	.050		
17	-.186	.700	.009	.710	-.769	.700		
19.0	-.182	1.310	.020	1.370	-.799	.059		
0	-.105	.002	-.034	.002				q=0

Run 12601
3 in. blades, q=10 psf

0	-.009	.005	-.007	.0026				q=0
0	306	.035	-.000	.030	.956	.008		
21	-.151	1.23	-.007	1.29	-.940	.027		

Table IV. Experimental Data, CCR Tests

Run 52605

Rotameter = 0.70, f = 9 Hz, q = 10.22 psf
Pressure (plenum) VRMS = 0.900
                  VDC = 5.500
Velocity   VRMS = 0.155
 (air sup. pipe) VDC = 1.000

Upper Surface			Lower Surface		
Tap no.	C_p Mean	RMS	Tap no.	C_p Mean	RMS
1	0.818	.119	29	-0.356	.472
2	0.131	.164	30	0.328	.125
3	0.012	.179	31	0.573	.104
4	-0.230	.209	32	0.600	.104
5	-0.699	.164	33	0.627	.113
6	-0.797	.164	34	0.600	.104
7	-0.694	.139	35	0.558	.104
8	-1.313	.134	36	0.487	.119
9	-1.119	.111	37	0.328	.125
10	-1.367	.119	38	0.256	.111
11	-1.331	.125	39	0.211	.111
12	-1.642	.119	40	0.181	.111
13	-1.797	.119	41	0.122	.111
14	-1.884	.119	42	0.075	.106
15	-1.916	.125	43	0.025	.111
16	-1.961	.134	44	-0.008	.111
17	-1.864	.139	45	0.000	.111
18	-1.976	.164	46	-0.008	.111
19	-1.844	.167	47	0.064	.111
20	-1.906	.181	48	0.014	.125
21	-1.936	.194	49	-0.136	.153
22	-2.056	.222	50	0.197	.153
23	-4.011	.514	51	0.406	.153
24	-5.972	.667	52	0.672	.139
25	-6.428	.903	53	0.903	.111
26	-5.331	.972	54	0.978	.083
27	-2.458	1.042			
28	-1.861	.889			
29	-0.356	.472			

Table IV. (cont'd)

Run 52604

Rotameter = 0.70, f = 0 Hz, q = 10.22 psf
Pressure (plenum) VRMS = 0.025
                   VDC = 0.025
Velocity   VRMS = 0.035
  (Air sup. pipe) VDC = 1.000

| Upper Surface | | | Lower Surface | | |
Tap no.	Mean	C_p RMS	Tap no.	Mean	C_p RMS
1	0.931	.080	29	-0.273	.273
2	0.631	.094	30	0.035	.096
3	0.000	.094	31	0.571	.086
4	0.014	.086	32	0.614	.080
5	-0.337	.086	33	0.620	.086
6	-0.437	.086	34	0.591	.080
7	-0.806	.082	35	0.549	.086
8	-0.889	.080	36	0.494	.086
9	-1.008	.082	37	0.336	.082
10	-1.191	.091	38	0.265	.082
11	-1.210	.082	39	0.224	.082
12	-1.389	.086	40	0.175	.082
13	-1.603	.086	41	0.115	.082
14	-1.717	.094	42	0.066	.082
15	-1.740	.086	43	0.033	.077
16	-1.803	.086	44	-0.071	.082
17	-1.779	.082	45	-0.057	.082
18	-1.903	.086	46	-0.019	.082
19	-1.803	.082	47	0.003	.082
20	-1.860	.082	48	-0.049	.082
21	-1.918	.082	49	-0.014	.082
22	-2.033	.082	50	0.169	.082
23	-4.011	.137	51	0.459	.082
24	-6.055	.137	52	0.661	.090
25	-6.262	.137	53	0.872	.082
26	-5.445	.546	54	0.981	.082
27	-2.413	.546			
28	-1.915	.464			
29	-0.273	.213			

Table IV. (cont'd)

Run 52603

Rotameter = 0.58, f = 9 Hz, q = 10.22 psf
Pressure (plenum)   VRMS = 1.100
                    VDC = 3.800
Velocity   VRMS = 0.240
  (air sup. pipe)   VDC = 1.000

Upper Surface	C_p		Lower Surface	C_p	
Tap no.	Mean	RMS	Tap No.	Mean	RMS
1	0.985	.103	29	0.104	.254
2	0.786	.117	30	0.335	.099
3	0.669	.176	31	0.446	.117
4	0.311	.176	32	0.457	.117
5	0.185	.161	33	0.475	.132
6	0.079	.161	34	0.443	.132
7	0.442	.155	35	0.425	.132
8	0.522	.147	36	0.355	.161
9	0.775	.141	37	0.211	.155
10	0.845	.132	38	0.076	.141
11	-1.107	.141	39	0.099	.141
12	-0.953	.132	40	0.070	.141
13	-1.164	.132	41	0.042	.127
14	-1.311	.147	42	0.017	.127
15	-1.381	.147	43	-0.076	.127
16	-1.411	.176	44	-0.124	.127
17	-1.470	.183	45	-0.149	.127
18	-1.455	.191	46	-0.146	.127
19	-1.499	.211	47	-0.070	.141
20	-1.417	.225	48	-0.034	.155
21	-1.490	.259	49	-0.115	.197
22	-1.577	.296	50	0.135	.197
23	-2.961	.676	51	0.237	.197
24	-4.479	1.042	52	0.304	.211
25	-4.282	1.211	53	0.780	.183
26	-3.631	1.388	54	0.997	.099
27	-1.155	.986			
28	-0.594	.704			
29	0.104	.254			

67

Table IV. (cont'd)

Run 52601

Rotameter = 0.58, f = 0 Hz, q = 10.22 psf
Pressure (plenum)   VRMS = 0.020
                    VDC = 3.800
Velocity   VRMS = 0.037
  (air sup. pipe)   VDC = 1.000

Upper Surface			Lower Surface		
Tap no.	Mean C_p	RMS	Tap no.	Mean C_p	RMS
1	1.018	.065	29	0.192	.028
2	0.762	.067	30	0.393	.097
3	0.194	.065	31	0.501	.067
4	0.032	.073	32	0.475	.073
5	-0.106	.073	33	0.446	.070
6	-0.358	.065	34	0.493	.067
7	-0.209	.070	35	0.440	.067
8	-0.692	.059	36	0.361	.065
9	-0.657	.064	37	0.212	.061
10	-0.971	.073	38	0.156	.056
11	-0.933	.064	39	0.125	.061
12	-1.229	.073	40	0.081	.064
13	-1.390	.073	41	0.008	.061
14	-1.490	.076	42	-0.006	.061
15	-1.540	.070	43	-0.103	.061
16	-1.575	.065	44	-0.167	.061
17	-1.482	.067	45	-0.195	.056
18	-1.604	.067	46	-0.170	.064
19	-1.468	.067	47	-0.203	.064
20	-1.476	.064	48	-0.248	.056
21	-1.462	.067	49	-0.337	.067
22	-1.585	.070	50	-0.220	.067
23	-2.997	.111	51	-0.042	.070
24	-4.724	.097	52	0.209	.072
25	-4.521	.125	53	0.462	.072
26	-3.713	.181	54	0.944	.064
27	-1.086	.334			
28	-0.599	.251			
29	0.192	.028			

Table IV. (cont'd)

Run 51002

Rotameter = 0.58, f = 0 Hz, q = 10.22 psf
Pressure (plenum)   VRMS = 0.022
                    VDC = 3.500
Velocity   VRMS = 0.022
  (air sup. pipe)   VDC = -.499

Upper Surface   Lower Surface

Tap no.	C_p	Tap no.	C_p
1	1.003	29	0.134
2	0.760	30	0.323
3	0.560	31	0.425
4	0.413	32	0.464
5	-0.012	33	0.449
6	-0.171	34	0.449
7	-0.372	35	0.419
8	-0.584	36	0.365
9	-0.709	37	0.125
10	-0.820	38	0.090
11	-0.983	39	0.064
12	-0.958	40	0.017
13	-1.177	41	-0.029
14	-1.323	42	-0.070
15	-1.362	43	-0.145
16	-1.416	44	-0.227
17	-1.471	45	-0.250
18	-1.488	46	-0.230
19	-1.468	47	-0.241
20	-1.474	48	-0.294
21	-1.494	49	-0.422
22	-1.500	50	-0.273
23	-2.869	51	-0.137
24	-4.488	52	0.058
25	-4.451	53	0.416
26	-3.535	54	0.860
27	-0.782		
28	-0.503		
29	-0.134		

Special Upper Surface Pressure

55	-1.131
56	-1.058
57	-0.968
58	-1.302
59	-1.102

Table IV. (cont'd)

Run 51003

Rotameter = 0.58, f = 9.1 Hz, q = 10.22 psf
Pressure (plenum)   VRMS = 0.500
                    VDC = 3.405
Velocity   VRMS = 0.601
  (air sup. pipe)   VDC = -.475

| Upper Surface | | | Lower Surface | | |
Tap no.	Mean C_p	RMS	Tap no.	C_p Mean	RMS
1	1.003	.074	29	0.165	.148
2	0.917	.080	30	0.353	.098
3	0.615	.098	31	0.435	.071
4	0.355	.112	32	0.459	.077
5	0.234	.118	33	0.441	.065
6	-0.101	.104	34	0.429	.080
7	-0.218	.101	35	0.405	.083
8	-0.524	.101	36	0.346	.083
9	-0.627	.098	37	0.165	.084
10	-0.805	.104	38	0.115	.078
11	-0.905	.101	39	0.073	.070
12	-0.982	.104	40	0.031	.070
13	-1.178	.104	41	-0.008	.070
14	-1.302	.104	42	-0.039	.078
15	-1.349	.104	43	-0.120	.073
16	-1.402	.121	44	-0.207	.076
17	-1.403	.123	45	-0.230	.078
18	-1.462	.121	46	-0.207	.070
19	-1.395	.123	47	-0.221	.076
20	-1.401	.134	48	-0.311	.073
21	-1.415	.148	49	-0.356	.101
22	-1.451	.154	50	-0.303	.115
23	-2.768	.345	51	-0.003	.112
24	-4.305	.513	52	0.081	.123
25	-4.249	.560	53	0.356	.126
26	-3.277	.630	54	0.835	.084
27	-0.745	.504			
28	-0.367	.406			
29	0.165	.148			

Special Upper Surface Pressures

55	-1.106	.098
56	-0.978	.092
57	-0.924	.092
58	-1.227	.112
59	-1.048	.104

70

REFERENCES

1. Charnay, G. and Mathieu, J. A., "Periodic Flow in a Wind Tunnel Produced by Rotating Shutters," _Journal of Fluids Engineering_, June 1976.

2. Coulson, C. A., _Waves, A Mathematical Account of the Common Types of Wave Motion_, Oliver and Boyd LTD, 1952.

3. Ingard, U. and Singhal, V. K., "Upstream and Downstream Sound Radiation into a Moving Fluid," _The Journal of the Acoustical Society of America_, v. 54, no. 5, p. 1343-1346, 1973.

4. Ingard, U. and Singhal, V. K., "Effect of Flow on the Acoustic Resonances of an Open-ended Duct," _The Journal of the Acoustical Society of America_, v. 58, no. 4, p. 788-793, October 1975.

5. Johnson, R. B., _A Technique for Measuring Unsteady Pressures_, Masters Degree Thesis, Naval Postgraduate School, September 1968.

6. Kail, K. A., Aeronautical Engineer Degree Thesis, Naval Postgraduate School, June 1977.

7. Kreyszig, E., _Advanced Engineering Mathematics_, John Wiley & Sons, Inc., 1972.

8. Murphy, J. C., _The Effects of Nonsteady Flow on the Pressure Distribution About a Circular Cylinder_, Aeronautical Engineer Degree Thesis, Naval Postgraduate School, May 1966.

9. Naval Postgraduate School Circulation Controlled Airfoil Research Program, _Progress Report, Circulation Control Airfoil Study_, by L. V. Schmidt and J. A. Miller, December 1975.

10. Naval Postgraduate School Circulation Controlled Airfoil Research Program, _Progress Report No. 3, Circulation Control Airfoil Study_, by L. V. Schmidt and J.A. Miller, December 1976.

11. Shapiro, A. H., _The Dynamics and Thermodynamics of Compressible Flow_, v. 1, The Ronald Press Company, 1953.

12. Simmons, J. M., "Measured Pressure Distributions on an Airfoil with Oscillating Jet Flap," _AIAA Journal_, v. 14, no. 9, p. 1297-1302, September 1976.

13. Zucrow, M. J. and Hoffman, J. D., Gas Dynamics, v. 1, John Wiley & Sons, Inc., 1976.

14. Miller, J. A., "A Simple Linearized Hot-Wire Anemometer," Journal of Fluids Engineering, v. 98, p. 749-752, December 1976.

INITIAL DISTRIBUTION LIST

No. Copies

1. Defense Documentation Center   2
   Cameron Station
   Alexandria, Virginia   22314

2. Library, Code 0142   2
   Naval Postgraduate School
   Monterey, California   93940

3. Department Chairman, Code 67   1
   Department of Aeronautics
   Naval Postgraduate School
   Monterey, California   93940

4. Professor L. V. Schmidt, Code 67Sx   1
   Department of Aeronautics
   Naval Postgraduate School
   Monterey, California   93940

5. Commanding Officer   1
   Attn: Mr. R. F. Siewert, AIR-320D
   Naval Air Systems Command
   Washington, D.C.   20361

6. Commanding Officer   2
   Attn: Dr. H. Chaplin, Code AESD
          Mr. J. Wilkerson, Code AESD
   David W. Taylor Naval Ship Research
      and Development Center
   Bethesda, Maryland   20084

7. Professor J. A. Miller, Code 67Mo   1
   Department of Aeronautics
   Naval Postgraduate School
   Monterey, California   93940

8. LT Emmett J. Lancaster, USN   1
   536 Manzanita Street
   Chula Vista, California 92011